ANTIMICROBIAL AGENTS AND CHEMOTHERAPY, Jan. 2008, p. 164–170 Vol. 52, No. 1
0066-4804/08/$08.00+0 doi:10.1128/AAC.00378-07

Anaerobic NADH-Fumarate Reductase System Is Predominant in the Respiratory Chain of *Echinococcus multilocularis*, Providing a Novel Target for the Chemotherapy of Alveolar Echinococcosis▽

Jun Matsumoto,[1] Kimitoshi Sakamoto,[2]* Noriko Shinjyo,[2] Yasutoshi Kido,[2] Nao Yamamoto,[1] Kinpei Yagi,[3] Hideto Miyoshi,[4] Nariaki Nonaka,[1] Ken Katakura,[1] Kiyoshi Kita,[2] and Yuzaburo Oku[1]

Laboratory of Parasitology, Department of Disease Control, Graduate School of Veterinary Medicine, Hokkaido University, Sapporo, Japan[1]; Department of Biomedical Chemistry, Graduate School of Medicine, University of Tokyo, Tokyo, Japan[2]; Department of Medical Zoology, Hokkaido Institute of Public Health, Sapporo, Japan[3]; and Division of Applied Life Sciences, Graduate School of Agriculture, Kyoto University, Kyoto, Japan[4]

Received 20 March 2007/Returned for modification 21 June 2007/Accepted 10 October 2007

Alveolar echinococcosis, which is due to the massive growth of larval *Echinococcus multilocularis*, is a life-threatening parasitic zoonosis distributed widely across the northern hemisphere. Commercially available chemotherapeutic compounds have parasitostatic but not parasitocidal effects. Parasitic organisms use various energy metabolic pathways that differ greatly from those of their hosts and therefore could be promising targets for chemotherapy. The aim of this study was to characterize the mitochondrial respiratory chain of *E. multilocularis*, with the eventual goal of developing novel antiechinococcal compounds. Enzymatic analyses using enriched mitochondrial fractions from *E. multilocularis* protoscoleces revealed that the mitochondria exhibited NADH-fumarate reductase activity as the predominant enzyme activity, suggesting that the mitochondrial respiratory system of the parasite is highly adapted to anaerobic environments. High-performance liquid chromatography–mass spectrometry revealed that the primary quinone of the parasite mitochondria was rhodoquinone-10, which is commonly used as an electron mediator in anaerobic respiration by the NADH-fumarate reductase system of other eukaryotes. This also suggests that the mitochondria of *E. multilocularis* protoscoleces possess an anaerobic respiratory chain in which complex II of the parasite functions as a rhodoquinol-fumarate reductase. Furthermore, in vitro treatment assays using respiratory chain inhibitors against the NADH-quinone reductase activity of mitochondrial complex I demonstrated that they had a potent ability to kill protoscoleces. These results suggest that the mitochondrial respiratory chain of the parasite is a promising target for chemotherapy of alveolar echinococcosis.

Echinococcosis is a near-cosmopolitan zoonosis caused by helminthic parasites belonging to the genus *Echinococcus* (family Taeniidae) (18). The life cycle of *Echinococcus* spp. includes an egg-producing adult stage in the definitive hosts and a larval stage in intermediate hosts including humans. The larval stage of the parasite produces a large number of infective protoscoleces that develop to adult worms after being ingested by the definitive host, or they produce a new parasite mass when liberated inside the intermediate host, causing metastases of the parasite lesions. The two major species of medical and public health importance are *Echinococcus granulosus* and *E. multilocularis*, which cause cystic echinococcosis and alveolar echinococcosis (AE), respectively.

Human AE is a life-threatening disease, and without careful clinical management, it has a high fatality rate and poor prognosis. Humans acquire AE infection by ingesting eggs from adult parasitic worms. Early diagnosis and treatment (mainly by radical surgery) of human AE are difficult because the disease progresses slowly and usually takes more than several years before clinical symptoms become apparent. An efficient chemotherapeutic compound is still not available. The first choice for the chemotherapy of AE is benzimidazole derivatives (18), but they are parasitostatic rather than parasitocidal against larval *E. multilocularis*. Therefore, the development of highly effective antiechinococcal drugs is urgently needed.

Biological systems for energy metabolism are essential for the survival, continued growth, and reproduction of all living organisms. "Typical" mitochondria are usually considered to be oxygen-consuming, ATP-producing organelles. In fact, typical mitochondria, such as those found in mammalian cells, require oxygen to function. They use pyruvate dehydrogenase for oxidative decarboxylation of pyruvate to acetyl coenzyme A, which is then completely oxidized to CO_2 through the Krebs cycle. Most of the energy is produced by oxidative phosphorylation: the electrons from NADH and succinate are transferred to oxygen by the proton-pumping electron transfer respiratory chain in which ubiquinone (UQ) (Fig. 1A) is commonly used as an electron mediator. The backflow of the protons results in ATP formation by the mitochondrial ATP synthase.

In parasitic organisms, on the other hand, the carbohydrate and energy metabolic pathways of adult parasitic helminths differ greatly from those of their vertebrate hosts. The most important factors in this respect are the nutrient and oxygen supply (reviewed in references 4, 12, and 13). Parasitic hel-

* Corresponding author. Mailing address: Department of Biomedical Chemistry, Graduate School of Medicine, University of Tokyo, Tokyo 113-0033, Japan. Phone: 81 3 58418202. Fax: 81 3 58413444. E-mail: sakamok@m.u-tokyo.ac.jp.

▽ Published ahead of print on 22 October 2007.

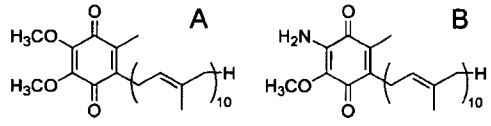

FIG. 1. Chemical structure of ubiquinone-10 (UQ_{10}) (E_m' = +110 mV) (A) and rhodoquinone-10 (RQ_{10}) (E_m' = −63 mV) (B).

minths have exploited a variety of energy-transducing systems during their adaptation to habitats in their hosts (7, 28). The parasitic nematode *Ascaris suum*, for example, resides in the host small intestine, where oxygen tensions are low, and exploits a unique anaerobic respiratory chain, called the NADH-fumarate reductase system, to adapt to its microaerobic habitat (Fig. 2) (2, 3, 14, 22; reviewed in reference 10). The NADH-fumarate reductase system is part of the unique respiratory system for parasitic helminthes and is the terminal step in the phosphoenolpyruvate carboxykinase-succinate pathway, which is found in many anaerobic organisms. Electrons from NADH are accepted by rhodoquinone (RQ) (Fig. 1B) via the NADH-RQ reductase activity of mitochondrial complex I and then transferred to fumarate through the rhodoquinol-fumarate reductase activity of mitochondrial complex II. The anaerobic electron transfer in complex I couples with proton transport across the mitochondrial inner membrane, providing ATP even in the absence of oxygen. This system, which does not normally function in mammalian mitochondria, is considered to be a good target for the development of novel anthelminthics (8, 9, 21). With regard to *Echinococcus* spp., the presence of both aerobic and anaerobic respiratory systems was previously suggested by a series of intensive studies (1, 16, 17), although the respiratory systems in this group of parasites are to be characterized in more detail.

In the present study, we prepared an enriched mitochondrial fraction from *E. multilocularis* protoscoleces and characterized the specific enzyme activities involved in mitochondrial energy metabolism as well as the quinone profile in the parasite's respiratory chain. Furthermore, based on findings reported previously by Yamashita et al. that quinazoline derivatives can inhibit the NADH-quinone reductase of mitochondria from *A. suum* (35), we tested several quinazoline-type compounds, with a view to developing novel antiechinococcal compounds.

MATERIALS AND METHODS

Isolation of *E. multilocularis* protoscoleces. We used the Nemuro strain of *E. multilocularis*, which is maintained at the Hokkaido Institute of Public Health (Sapporo, Japan). Mature larval parasites with protoscolex formation were obtained from cotton rats (*Sigmodon hispidus*) more than 4 months after oral infection with 50 parasite eggs. To isolate protoscoleces, the mature larval parasites were minced with scissors, pushed through a metal mesh, and washed repeatedly with physiological saline until host materials were thoroughly removed.

Preparation of enriched mitochondrial fractions. The enriched mitochondrial fractions of *E. multilocularis* protoscoleces were prepared essentially according to methods described previously for isolating adult *Ascaris* mitochondria (25, 26). Briefly, the isolated protoscolex sediment was suspended in 5 volumes of mitochondrial preparation buffer (210 mM mannitol, 10 mM sucrose, 1 mM disodium EDTA, and 50 mM Tris-HCl [pH 7.5]) supplemented with 10 mM sodium malonate. The parasite materials were homogenized with a motor-driven glass/glass homogenizer (six passes three to four times). The homogenate was diluted with the mitochondrial preparation buffer to 10 times the volume of the original protoscolex sediment and then centrifuged at 800 × *g* for 10 min to precipitate cell debris and nuclei. The supernatant was then centrifuged at 8,000 × *g* for 10 min to obtain the mitochondrial pellet. The pellet was resuspended in mitochondrial preparation buffer (without malonate) and centrifuged at 12,000 × *g* for 10 min. The resulting enriched mitochondrial fraction was suspended in mitochondrial preparation buffer (without malonate). The protein concentration was determined according to the method of Lowry et al. by using bovine serum albumin as a standard (15).

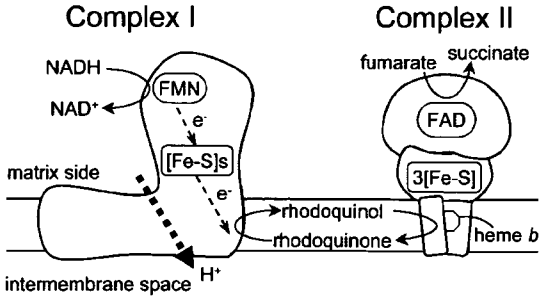

FIG. 2. Schematic representation of the NADH-fumarate reductase system in adult *A. suum*, which catalyzes the final step of the phosphoenolpyruvate carboxykinase-succinate pathway. In this system, the reducing equivalent of NADH is transferred to the low-potential RQ by the NADH-RQ reductase activity of mitochondrial complex I. This pathway ends with the production of succinate by the rhodoquinol-fumarate reductase activity of complex II. Electron transfer from NADH to fumarate is coupled to the site I phosphorylation of complex I via the generation of a proton-motive force. FMN, flavin mononucleotide; FAD, flavin adenine dinucleotide; [Fe-S]s and 3[Fe-S], iron-sulfur clusters.

Western blotting. An enriched mitochondrial fraction prepared from *E. multilocularis* protoscoleces and that from the liver of a cotton rat (used as the host animal for the parasite) were analyzed by Western blotting. Reactions were performed according to a method described previously by Towbin et al. (30). The proteins were separated by sodium dodecyl sulfate-polyacrylamide gel electrophoresis on a 10% or 15% acrylamide gel and electrophoretically transferred onto a nitrocellulose membrane. The membrane was soaked in 1:5,000 anti-cytochrome *c* oxidase subunit IV antibody (component of the ApoAlert cell fractionation kit; Clontech Laboratories) in phosphate-buffered saline containing 0.05% (wt/vol) Tween 20 and 2% (wt/vol) skim milk. The membrane was incubated for 60 min at room temperature and then washed three times for 10 min with washing buffer, which consisted of 0.05% (wt/vol) Tween 20 in phosphate-buffered saline. Alkaline phosphatase-conjugated goat anti-mouse immunoglobulin G was then added as a secondary antibody, and the mixture was incubated for 30 min. After another wash with washing buffer, the membrane was soaked in reaction buffer (100 mM Tris-HCl [pH 9.5], 100 mM NaCl, 5 mM $MgCl_2$, 500 μg/ml of 4-nitroblue tetrazolium chloride, and 165 μg/ml of 5-bromo-4-chloro-3-indolylphosphate) to initiate the development of a colored product. Finally, the membrane was washed with distilled water to stop the reaction. For Western blotting, the amounts of parasite and cotton rat mitochondrial samples were normalized by the total protein amount or cytochrome *c* oxidase activity (see below).

Enzyme assays. All enzyme assays using the enriched mitochondrial fractions were performed in a 0.7- or 1-ml reaction mixture at 25°C. The reagents used in each assay were mixed with reaction buffer containing 30 mM potassium phosphate (pH 7.4) and 1 mM $MgCl_2$. The final mitochondrial protein concentration was 80 μg per ml of reaction mixture. For all reactions performed under anaerobic conditions, the reaction medium was supplemented with 100 μg/ml glucose oxidase, 2 μg/ml catalase, and 10 mM β-D-glucose and left for 3 min to achieve anaerobiosis. NADH oxidase activity in the isolated mitochondrial fraction was determined in the presence or absence of 2 mM KCN, 100 mM malonate, or both by measuring the absorbance of NADH at 340 nm (ε = 6.2 mM^{-1} cm^{-1}). The reaction was initiated by the addition of 100 μM of NADH to the mixture. Succinate dehydrogenase (SDH) activity was determined by monitoring the absorbance change of 2-(4,5-dimethyl-2-thiazolyl)-3,5-diphenyl-2*H*-tetrazolium bromide (MTT; 60 μg/ml) at 570 nm in the presence of 120 μg/ml phenazine methosulfate and 2 mM KCN. The reaction was initiated by the addition 10 mM of succinate to the mixture. Succinate-quinone reductase activity was assayed under aerobic or anaerobic conditions in the presence of 0.1%(wt/vol) sucrose monolaurate by determining the amount of decyl UQ (dUQ) or decyl RQ (dRQ)

from the absorbance change at 278 nm (ε = 12.7 mM^{-1} cm^{-1}) or 287 nm (ε = 9.2 mM^{-1} cm^{-1}), respectively. Decyl rhodoquinol-fumarate reductase activity was measured under anaerobic conditions in a reaction mixture containing 0.1% (wt/vol) sucrose monolaurate. In this reaction, 60 μM dRQ was reduced to decyl rhodoquinol in the cuvette by adding 200 μM $NaBH_4$. The reaction was started by adding 5 mM fumarate to the mixture, and the oxidation of decyl rhodoquinol was monitored at 287 nm. NADH-fumarate reductase activity was determined by monitoring the oxidation of NADH (100 μM) at 340 nm under anaerobic conditions. The reaction was initiated by the addition of 5 mM fumarate as an electron acceptor. NADH-quinone reductase activity assays were carried out under anaerobic conditions using the same reaction mixture as that used for the NADH-fumarate reductase activity assay except that 60 μM dUQ or dRQ was used as an electron acceptor instead of fumarate. The enzyme activity was determined by monitoring the absorbance change of NADH at 340 nm. Ubiquinol oxidase activity was determined by monitoring the absorbance change of ubiquinol-1 (150 μM) at 278 nm (ε = 12.7 mM^{-1} cm^{-1}) in the presence or absence of 2 mM KCN. The activity of cytochrome *c* oxidase was determined as *N,N,N′,N′*-tetramethyl-*p*-phenylenediamine dihydrochloride (TMPD) oxidase activity, which was measured by monitoring the absorbance change of TMPD (500 μM) at 610 nm (ε = 11.0 mM^{-1} cm^{-1}) in the presence or absence of 2 mM KCN.

Enzyme inhibition assays. Based on the findings of Yamashita et al. showing that that quinazoline-type compounds inhibit the NADH-quinone reductase activity of *A. suum* complex I (35), we determined 50% inhibitory concentration (IC_{50}) values of the quionazoline-type compounds against NADH-fumarate reductase activity of the parasite mitochondria and the NADH oxidase activity of bovine heart mitochondria (see "Enzyme assays"). The compounds used in the assays included quinazoline and its derivatives 6-NH_2, 6-$NHCO(CH{=}CH_2)$, 7-NH_2, 8-OH, 8-OCH_3, 8-OCH_2CH_3, and 8-$OCH(CH_3)_2$.

Analysis of the quinone profile of isolated mitochondria. Quinones were extracted from lyophilized mitochondria essentially according to a method described previously by Takada et al. (24). A lyophilized mitochondrial sample (2.9 mg protein) was crushed into powder before extraction, vortexed in 2:5 (vol/vol) ethanol/*n*-hexane for 10 min, and centrifuged at 20,000 × *g* for 5 min at room temperature. The supernatants were pooled, and the extraction of quinones was repeated twice. Pooled extracts were evaporated to dryness, dissolved in ethanol, and kept in the dark until high-performance liquid chromatography (HPLC) analysis. Quinones were applied to a reverse-phase HPLC column (Inertsil ODS-3 [5 μm and 4.6 by 250 mm]; GL Science) and eluted under isocratic conditions (1 ml/min) with 1:4 (vol/vol) diisopropyl ether-methanol at 25°C. The molecular species of the eluted quinones were identified by their retention times and by their spectral characteristics as measured with a UV-visible photodiode array (Shimadzu SPD-10-A). The concentration of quinones was determined spectrophotometrically. The major quinone detected was confirmed by mass spectrometry (MS) using an Applied Biosystems API-165 LC/MS system with electrospray ionization.

In vitro treatment of *E. multilocularis* protoscoleces. *E. multilocularis* protoscoleces were obtained as described above (see "Isolation of *E. multilocularis* protoscoleces"). The parasite materials were placed into culture medium suitable for the long-term maintenance of the protoscoleces in vitro (27). The parasite cultures were kept in a six-well plate at a density of approximately 500 protoscoleces per ml of culture medium, and half of the medium was replaced twice a week. This culture condition was also applied during in vitro treatment of the parasite. To examine the efficacy of chemical compounds against living *E. multilocularis* protoscoleces, the parasites were kept in the culture medium supplemented with 5 or 50 μM of each compound, including quinazoline and its 8-OH derivative, rotenone (a specific inhibitor of mitochondrial complex I) (19) and nitazoxanide (a compound with strong protoscolicidal action) (32). One control group was supplemented with 0.5% (vol/vol) dimethyl sulfoxide (vehicle) alone, and all conditions were assayed in triplicate. The viability of protoscoleces was determined by microscopic analysis of more than 170 protoscoleces per well for motile behavior and the ability to exclude trypan blue (32).

RESULTS

Preparation of enriched mitochondrial fractions. To characterize the mitochondrial respiratory chain of *E. multilocularis* protoscoleces, we prepared enriched mitochondrial fractions from the parasite. Approximately 80 g of larval *E. multilocularis* (containing approximately 10^5 protoscoleces per gram) was obtained from each cotton rat more than 4 months after oral infection with 50 parasite eggs. Approximately 20 g of the larval parasite was used per isolation of protoscoleces, yielding 2 ml of cleaned protoscolex sediment (Fig. 3). The enriched mitochondrial fractions were prepared from the protoscolex sediment as described in Materials and Methods. Each 1 ml of protoscolex sediment (containing 4.5 × 10^5 protoscoleces) yielded approximately 4 mg of mitochondria. Western blotting using an antibody to mammalian cytochrome *c* oxidase detected a specific band in the mitochondria from the liver of a cotton rat but not in mitochondria from *E. multilocularis* protoscoleces even when the amounts of both mitochondrial samples were normalized according to cytochrome *c* oxidase activity (data not shown). These results demonstrated that the enriched mitochondrial fractions from the parasite were sufficiently free of host components for use in enzyme assays and quinone analyses. In order to assess the quality of mitochondria, intactness was examined by the reactivity of NADH, which is a non-membrane-permeable substrate. NADH oxidase activity was not detected in the isotonic buffer, whereas it was fully activated in hypotonic buffer after a freeze-thaw treatment of the enriched mitochondrial fraction. Based on the results obtained, the method applied here for mitochondrial preparation seemed to be appropriate.

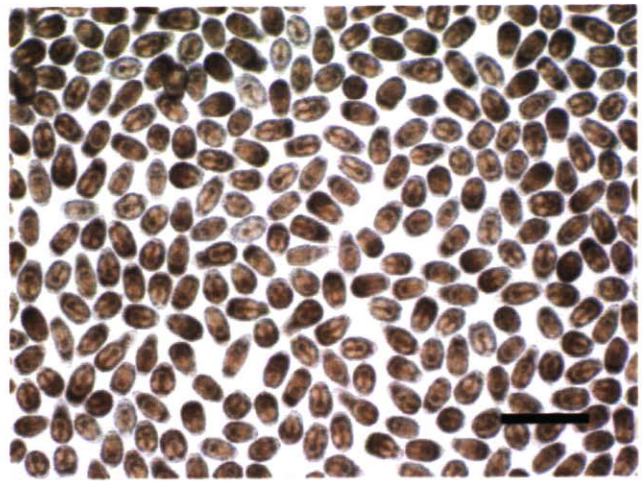

FIG. 3. Protoscoleces of *E. multilocularis* (Nemuro strain) used for the preparation of enriched mitochondrial fractions of the parasite and subsequent analyses. Bar, 500 μm.

Enzyme activities of *E. multilocularis* mitochondria. The specific enzyme activities involved in the mitochondrial respiratory chain of *E. multilocularis* protoscoleces are shown in Table 1. Parasite complex II exhibited an SDH activity of 103 nmol/min/mg. The specific activity of succinate-dUQ reductase was comparable to that of SDH activity (98.9 nmol/min/mg), whereas the succinate-dRQ reductase activity was lower (16.6 nmol/min/mg). The specific activity of decyl rhodoquinol-fumarate reductase, which is the reverse reaction of the succinate-RQ reductase activity of complex II, was determined to be 60.2 nmol/min/mg. The mitochondria of *E. multilocularis* protoscoleces exhibited NADH oxidase activity of 9.1 nmol/min/mg, which was almost eliminated by 2 mM KCN and 100 mM malonate. Ubiquinol-1 oxidase and TMPD oxidase activities were determined to be 4.4 nmol/min/mg and 12.6 nmol/

TABLE 1. Specific activities of mitochondrial respiratory enzymes in *E. multilocularis* protoscoleces

Assay	Sp act[a] (nmol/min/mg of protein) (mean ± SD)
SDH	103 ± 16
Succinate-quinone reductase	
dUQ (anaerobic)	98.9 ± 12
dRQ (anaerobic)	16.6 ± 3.5
Quinol-fumarate reductase (decyl rhodoquinol) (anaerobic)	60.2 ± 18
NADH oxidase	9.1 ± 2.1
NADH oxidase with:	
2 mM KCN	7.3 ± 1.5
100 mM malonate	4.4 ± 0.4
2 mM KCN and 100 mM malonate	1.7 ± 0.7
Ubiquinol-1 oxidase	4.4 ± 0.6
TMPD oxidase	12.6 ± 6.3
NADH-fumarate reductase (anaerobic)	45.0 ± 8.1
NADH-quinone reductase	
dUQ (anaerobic)	32.1 ± 2.7
dRQ (anaerobic)	61.3 ± 4.3

[a] Specific activities were obtained from at least three independently isolated mitochondria.

min/mg, respectively. These activities were completely inhibited by 2 mM KCN. Under anaerobic conditions, the specific activity of NADH-fumarate reductase was 45 nmol/min/mg, which was much higher than the NADH oxidase activity. The specific activity of NADH-dUQ reductase and NADH-dRQ reductase of complex I were determined to be 32.1 and 61.3 nmol/min/mg, respectively.

Quinone components in *E. multilocularis* mitochondria. To determine which quinones act as physiological electron mediators in the mitochondrial respiratory system of *E. multilocularis* protoscoleces, HPLC analyses were performed. As shown in Fig. 4A, the enriched mitochondrial fractions contained only one major quinone component at a retention time (*Rt*) of 22.4 min. The peak fraction exhibited a characteristic absorption maximum for RQs at 283 nm (Fig. 4B) (20). Subsequent MS analysis confirmed that the primary quinone of the parasite was RQ_{10} (electrospray ionization-MS *m/z* 848.8 $[M + H]^+$). The concentration of RQ_{10} was determined to be 0.73 nmol/mg of mitochondrial protein.

Effects of inhibitors on NADH-fumarate reductase in *E. multilocularis* mitochondria. To investigate the inhibitory effect of quinazoline (Fig. 5A) and its derivatives on the enzymatic activities in the anaerobic respiratory system of *E. multilocularis* mitochondria, we determined IC_{50} values against the NADH-fumarate reductase activity of the enriched mitochondrial fraction of the parasite. We found that all of the compounds inhibited the NADH-fumarate reductase activity of the parasite to some extent. Quinazoline and its derivatives including 6-NH_2, 6-NHCO(CH=CH_2), 7-NH_2, 8-OH, 8-OCH_3, 8-OCH_2CH_3, and 8-$OCH(CH_3)_2$ exhibited IC_{50} values of 2.3, 2.1, 16, 62, 71, 48, 4,100, and 910 nM, respectively. Of the compounds tested, the 8-OH derivative (Fig. 5B) exhibited relatively selective inhibition against the NADH-fumarate reductase activity of *E. multilocularis* protoscoleces compared with the NADH oxidase activities of mammalian mitochondria: the IC_{50} values of quinazoline and its 8-OH derivative for

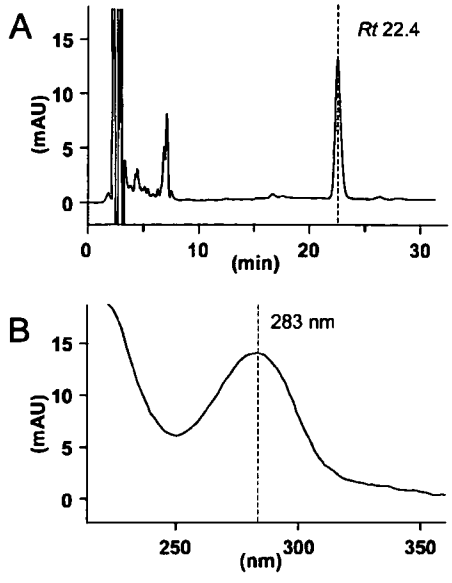

FIG. 4. (A) HPLC analysis of quinones extracted from the enriched mitochondrial fraction of *E. multilocularis* protoscoleces. Detailed experimental conditions are described in Materials and Methods. The highest peak had a retention time of 22.4 min (arrow). (B) Absorption of this peak was 283 nm, suggesting that it contained an RQ. mAU, milli-absorbance units.

the NADH oxidase activities of mammalian (bovine heart) mitochondria were 0.40 and 230 nM, respectively.

Effects of inhibitors on living *E. multilocularis* protoscoleces. In order to examine the parasite-killing activities of the quinazoline-type compounds with different degrees of inhibitory effects against NADH-fumarate activities of *E. multilocularis* protoscoleces, we performed in vitro treatment of the parasite using quinazoline and its 8-OH derivative. The viability of the *E. multilocularis* protoscolex was progressively reduced during in vitro treatment of the parasites with 50 μM of the 8-OH derivative, and by day 5, all the parasites died (Fig. 6). The same compound did not have an obvious antiparasitic effect when used at a concentration of 5 μM. On the other hand, nonsubstituted quinazoline, which showed lower IC_{50} values with the enzymatic assay, eliminated the parasites on days 5 and 7 of in vitro treatment when used at 50 and 5 μM, respectively. Treatment with rotenone, a specific inhibitor of mitochondrial complex I (19), affected the viability of the parasite in a manner similar to that of the 8-OH derivative. The anti-echinococcal effect of nitazoxanide was relatively mild: even in

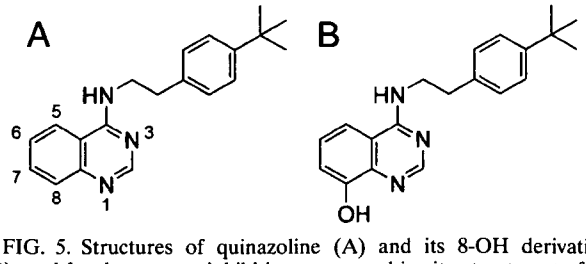

FIG. 5. Structures of quinazoline (A) and its 8-OH derivative (B) used for the enzyme inhibition assays and in vitro treatment of *E. multilocularis* protoscoleces.

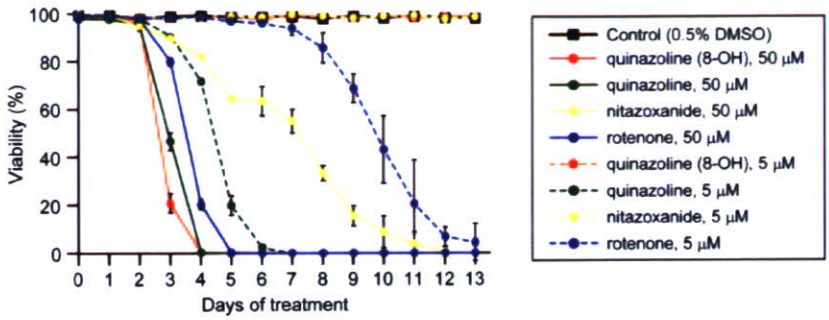

FIG. 6. Viability of *E. multilocularis* protoscoleces during in vitro treatment with quinazoline and its 8-OH derivatives, rotenone and nitazoxanide. Each compound was added to the culture medium at 5 or 50 μM. The results represent the means ± standard deviations of at least triplicate samples. DMSO, dimethyl sulfoxide.

the presence of 50 μM nitazoxanide, the viability decreased, but it did so only gradually, and it took 13 days before all the protoscoleces died. This compound did not affect parasite viability when used at 5 μM.

DISCUSSION

The most notable finding of the present study is that *E. multilocularis* protoscoleces possess a unique mitochondrial respiratory system that is highly adapted to anaerobic conditions. Specifically, the predominant enzymatic activity in the enriched mitochondrial fraction prepared from the parasite protoscoleces is the NADH-fumarate reductase system, which does not normally function in the aerobic respiratory chain of mammals. Thus, we infer that mitochondrial respiratory system of *E. multilocularis* would be a good target for the development of novel selective antiechinococcal compounds as demonstrated previously for other helminthic diseases (8, 21).

As early as 1957, Agosin found that *E. granulosus* protoscoleces have both aerobic and anaerobic respiratory systems and that glycolytic inhibitors are effective against both of them, indicating that they both depend on glycolysis (1). Subsequently, McManus and Smyth observed that protoscoleces cultured under anaerobic conditions produce more succinate than parasites kept under aerobic conditions, suggesting that the parasites survive under anaerobic conditions by utilizing the NADH-fumarate reductase system (16). Furthermore, McManus and Smyth reported that the specific activity of fumarate reductase in *Echinococcus* protoscoleces is lower than those of enzymes involved in the tricarboxylic acid cycle (17). These results, however, did not establish the importance of NADH-fumarate reductase activity in the mitochondrial respiratory system of the parasite because the other enzyme activities were not analyzed.

In the present study, we focused on the enzyme activities of the mitochondrial respiratory system of the parasite to determine whether the system is adapted to anaerobic conditions. Using the enriched mitochondrial fractions prepared from *E. multilocularis* protoscoleces, we showed that the activity of NADH-fumarate reductase in the respiratory system of the parasite is predominant compared with that of NADH oxidase, an enzyme involved in aerobic respiration in aerobic organisms such as mammals. Furthermore, direct measurements of complex II activities in both directions (i.e., succinate-RQ reductase and rhodoquinol-fumarate reductase activities) indicated that parasite complex II functions more favorably as a rhodoquinol-fumarate reductase in the presence of RQ/rhodoquinol. Thus, our results using isolated mitochondria of *E. multilocularis* protoscoleces coupled with assay systems for the determination of the parasite's enzyme activities revealed for the first time that the parasite mitochondria are highly adapted to anaerobic environments.

Analyses of the quinone components of *E. multilocularis* mitochondria revealed that RQ_{10} (Fig. 1B), whose redox potential is much more negative (E_m' [midpoint potential] = −63 mV) than that of UQ_{10} (E_m' = +110 mV) (Fig. 1A), was the primary quinone component of parasite mitochondria. In other parasitic helminths, like *A. suum* and *Hymenolepis diminuta*, RQ is an essential component of the NADH-fumarate reductase system (5, 11). In addition, van Hellemond et al. previously demonstrated that for all eukaryotes, the relative amount of RQ compared to the total amount of quinones correlates well with the importance of fumarate reduction in vivo (31). Similarly, during the development of the liver fluke *Fasciola hepatica*, there is a good correlation between the quinone composition and the importance of fumarate reduction in vivo (31). Therefore, RQ seems to be an essential component of fumarate reduction in eukaryotic respiration. Although menaquinone-related fumarate reduction in prokaryotes is well known (33, 34), there is no evidence that menaquinone serves this function in eukaryotes. In this study, enzyme assays demonstrated that the mitochondria from *E. multilocularis* possess NADH-fumarate activity as the predominant activity. In addition, the NADH-dRQ reductase activity was much higher than that of NADH-dUQ reductase, indicating that *E. multilocularis* complex I may interact preferentially with RQ rather than with UQ. Taken together, these results indicate that, as in other metazoan eukaryotes with anaerobic respiratory systems, *E. multilocularis* protoscoleces have a unique respiratory system that is highly adapted to anaerobic environments and in which RQ_{10} is used as the primary electron mediator.

Spiliotis et al. recently reported that the in vitro growth of larval *E. multilocularis* is more active under anaerobic than aerobic conditions (23). Thus, our findings for the respiratory system of *E. multilocularis* protoscoleces are consistent with the observations reported previously by Spiliotis et al. Larval *E. multilocularis* containing a large number of protoscoleces

lives in host tissues, mainly the liver, surrounded by thick connective tissues containing carbohydrate-rich laminated layers, which probably provide the parasite cells with an extremely-low-oxygen environment. Accordingly, it is not surprising that the parasite survives in the host by utilizing an anaerobic respiratory system.

Many anaerobic parasitic eukaryotes use the NADH-fumarate pathway, which is absent in mammals (2, 3, 10, 14, 22, 29). Therefore, this unique respiratory system is regarded as a promising chemotherapeutic target for the development of novel anthelminthics, as discussed in a recent review (9). In fact, Omura et al. previously found a natural compound, nafuredin, that is a potent inhibitor of the adult *A. suum* mitochondrial respiratory chain but much weaker against the mammalian mitochondrial respiratory chain (21). Yamashita et al. also found that quinazoline-type inhibitors were highly effective against adult *A. suum* complex I (35). Kinetic analyses using a series of quinazoline-type inhibitors revealed that *A. suum* complex I recognizes RQ_2 or UQ_2 in different ways, suggesting that mitochondrial complex I, which reacts preferably with RQs, could be a good target for chemotherapy. In the present study, we also tested several quinazoline-type compounds for their abilities to inhibit the anaerobic respiratory system of *E. multilocularis* protoscoleces. We found that all of the quinazoline-type compounds inhibited the NADH-fumarate reductase activity of *E. multilocularis* mitochondria to different extents. Furthermore, these compounds exhibited potent parasite-killing activities against *E. multilocularis* protoscoleces under in vitro culture conditions. Importantly, the nonsubstituted quinazoline, which has a higher inhibitory effect against NADH-fumarate oxidoreductase of the parasite mitochondria than the 8-OH derivative does, exhibited the parasite-killing activity even when used at 5 μM, whereas the 8-OH derivative did not do so at the same concentration. Such a correlation between the enzyme inhibition and the parasite-killing activities of these compounds suggests that the anaerobic NADH-fumarate reductase system of the parasite is a promising target for the development of antiechinococcal drugs.

Antiechinococcal drugs for chemotherapy of human AE should target not only protoscoleces but also the germinal layers of the *E. multilocularis* metacestode. The germinal layers in the larval parasite exhibit extremely unique characteristics. The parasite cells forming the germinal layers can differentiate into various tissues, including brood capsules and protoscoleces, and at the same time, they proliferate asexually as they remain in an undifferentiated state. This causes enlargement and, occasionally, metastasis of the lesions due to the formation of a large parasite mass. Therefore, for chemotherapy of AE, a complete cure cannot be achieved unless the germinal cells of the larval parasite are eliminated. Therefore, the mitochondrial respiratory system of germinal cells should be further characterized to aid in the development of a novel antiechinococcal compound(s) targeting the energy metabolism of larval *E. multilocularis*. However, it is presently quite difficult to obtain enough metacetode materials with homogeneous quality. Established methodologies for the in vitro cultivation of *E. multilocularis* metacestodes are now available (6, 23), and they will hopefully be applicable to large-scale preparations of metacestode materials in the near future.

During the life cycle of *E. multilocularis*, the parasite never undergoes active development and/or energy metabolism under aerobic conditions. The larval parasite lives mainly in the liver of intermediate host animals, whereas the adult worm dwells inside the small intestine of the final host, both of which are microaerobic conditions. Although the eggs of the parasite are exposed to air, they already contain a mature infective larva (oncosphere) waiting to be taken up by the next intermediate host. Therefore, the oncosphere does not develop or move under aerobic conditions. Taken together, these findings suggest that the respiratory system of *E. multilocularis* protoscoleces, as characterized in the present study, could represent the respiratory system used by the parasite throughout its developmental stages. Based on this speculation, the use of protoscolex materials in the first-step screening of candidate compounds by enzyme inhibition assays and subsequent in vitro parasite-killing assays appears to be reasonable, although it should be confirmed that the respiratory system of the *E. multilocularis* metacestode shares the same basic characteristics with that of the protoscolex stage of the parasite. We have already done preliminary experiments on the effects of the compounds used in this study, including the quinazoline derivative (8-OH), against in vitro-cultured metacestodes and found that the compounds exhibited high parasite-killing activities as evaluated by a modified MTT assay (data not shown). These results strongly suggest that our strategy is appropriate.

Highly effective chemotherapeutic compounds against human AE are not currently available despite the fact that the disease can be lethal unless the patient is appropriately treated during the early stage of the infection. Based on the findings presented here, it appears that the anaerobic respiratory system of *E. multilocularis*, which is distinct from that of host mammals, is a good target for the development of highly effective antiechinococcal drugs and, furthermore, that respiratory chain inhibitors (21, 35) are possible lead compounds for the development of antiechinococcal drugs.

ACKNOWLEDGMENTS

We thank Andrew Hemphill at the University of Berne for kindly providing us with precious chemical compounds.

This work was supported by grants from the following organizations: the Ministry of Education, Culture, Sports, Science, and Technology of Japan for the 21st Century COE Program, Program of Excellence for Zoonosis Control, and 18073004; the Ministry of Health and Welfare, Japan, for the Control of Emerging and Reemerging Diseases in Japan; the Japan Society of the Promotion of Science (grants 17790274 and 18GS0314); the Northern Advancement Center for Science and Technology; and the Akiyama Foundation.

REFERENCES

1. **Agosin, M.** 1957. Studies on the metabolism of *Echinococcus granulosus*. II. Some observations on the carbohydrate metabolism of hydatid cyst scolices. Exp. Parasitol. **6**:586–593.
2. **Amino, H., A. Osanai, H. Miyadera, N. Shinjyo, T. Tomitsuka, H. Taka, R. Mineki, K. Murayama, S. Takamiya, T. Aoki, H. Miyoshi, K. Sakamoto, S. Kojima, and K. Kita.** 2003. Isolation and characterization of the stage-specific cytochrome *b* small subunit (CybS) of *Ascaris suum* complex II from the aerobic respiratory chain of larval mitochondria. Mol. Biochem. Parasitol. **128**:175–186.
3. **Amino, H., H. Wang, H. Hirawake, F. Saruta, D. Mizuchi, R. Mineki, N. Shindo, K. Murayama, S. Takamiya, T. Aoki, S. Kojima, and K. Kita.** 2000. Stage-specific isoforms of *Ascaris suum* complex. II. The fumarate reductase of the parasitic adult and the succinate dehydrogenase of free-living larvae share a common iron-sulfur subunit. Mol. Biochem. Parasitol. **106**:63–76.
4. **Bryant, C., and C. Behm.** 1989. Energy metabolism, p. 25–69. *In* C. Bryant

and C. Behm (ed.), Biochemical adaptation in parasites. Chapman and Hall, London, United Kingdom.
5. **Fioravanti, C. F., and Y. Kim.** 1988. Rhodoquinone requirement of the *Hymenolepis diminuta* mitochondrial electron transport system. Mol. Biochem. Parasitol. **28**:129–134.
6. **Hemphill, A., and B. Gottstein.** 1995. Immunology and morphology studies on the proliferation of in vitro cultivated *Echinococcus multilocularis* metacestodes. Parasitol. Res. **81**:605–614.
7. **Kita, K., H. Hirawake, and S. Takamiya.** 1997. Cytochromes in the respiratory chain of helminth mitochondria. Int. J. Parasitol. **27**:617–630.
8. **Kita, K., C. Nihei, and E. Tomitsuka.** 2003. Parasite mitochondria as drug target: diversity and dynamic changes during the life cycle. Curr. Med. Chem. **10**:2535–2548.
9. **Kita, K., K. Shiomi, and S. Omura.** 2007. Advances in drug discovery and biochemical studies. Trends Parasitol. **23**:223–229.
10. **Kita, K., and S. Takamiya.** 2002. Electron-transfer complexes in *Ascaris* mitochondria. Adv. Parasitol. **51**:95–131.
11. **Kita, K., S. Takamiya, R. Furushima, Y. Ma, H. Suzuki, T. Ozawa, and H. Oya.** 1988. Electron-transfer complexes of *Ascaris suum* muscle mitochondria. III. Composition and fumarate reductase activity of complex II. Biochim. Biophys. Acta **935**:130–140.
12. **Köhler, P.** 1991. The pathways of energy generation in filarial parasites. Parasitol. Today **7**:21–25.
13. **Komuniecki, R., and B. G. Harris.** 1995. Carbohydrate and energy metabolism in helminths, p. 49–66. *In* J. J. Marr and M. Müller (ed.), Biochemistry and molecular biology of parasites. Academic Press, New York, NY.
14. **Kuramochi, T., H. Hirawake, S. Kojima, S. Takamiya, R. Furushima, T. Aoki, R. Komuniecki, and K. Kita.** 1994. Sequence comparison between the flavoprotein subunit of the fumarate reductase (complex II) of the anaerobic parasitic nematode, *Ascaris suum* and the succinate dehydrogenase of the aerobic, free-living nematode, *Caenorhabditis elegans*. Mol. Biochem. Parasitol. **68**:177–187.
15. **Lowry, O. H., N. J. Rosebrough, A. L. Farr, and R. J. Randall.** 1951. Protein measurement with the Folin phenol reagent. J. Biol. Chem. **193**:265–275.
16. **McManus, D. P., and J. D. Smyth.** 1978. Differences in the chemical composition and carbohydrate metabolism of *Echinococcus granulosus* (horse and sheep strains) and *E. multilocularis*. Parasitology **77**:103–109.
17. **McManus, D. P., and J. D. Smyth.** 1982. Intermediary carbohydrate metabolism in protoscoleces of *Echinococcus granulosus* (horse and sheep strains) and *E. multilocularis*. Parasitology **84**:351–366.
18. **McManus, D. P., W. Zhang, J. Li, and P. B. Bartley.** 2003. Echinococcosis. Lancet **362**:1295–1304.
19. **Miyoshi, H.** 1998. Structure-activity relationships of some complex I inhibitors. Biochim. Biophys. Acta **1364**:236–244.
20. **Moore, H. W., and K. Folkers.** 1965. Coenzyme Q. LXII. Structure and synthesis of rhodoquinone, a natural aminoquinone of the coenzyme Q group. J. Am. Chem. Soc. **87**:1409–1410.
21. **Omura, S., H. Miyadera, H. Ui, K. Shiomi, Y. Yamaguchi, R. Masuma, T. Nagamitsu, D. Takano, T. Sunazuka, A. Harder, H. Kölbl, M. Namikoshi, H. Miyoshi, K. Sakamoto, and K. Kita.** 2001. An anthelmintic compound, nafuredin, shows selective inhibition of complex I in helminth mitochondria. Proc. Natl. Acad. Sci. USA **98**:60–62.
22. **Saruta, F., T. Kuramochi, K. Nakamura, S. Takamiya, Y. Yu, T. Aoki, K. Sekimizu, S. Kojima, and K. Kita.** 1995. Stage-specific isoforms of complex II (succinate-ubiquinone oxidoreductase) in mitochondria from the parasitic nematode, *Ascaris suum*. J. Biol. Chem. **270**:928–932.
23. **Spiliotis, M., D. Tappe, L. Sesterhenn, and K. Brehm.** 2004. Long-term in vitro cultivation of *Echinococcus multilocularis* metacestodes under axenic conditions. Parasitol. Res. **92**:430–432.
24. **Takada, M., S. Ikenoya, T. Yuzuriha, and K. Katayama.** 1982. Studies on reduced and oxidized coenzyme Q (ubiquinones). II. The determination of oxidation-reduction levels of coenzyme Q in mitochondria, microsomes and plasma by high-performance liquid chromatography. Biochim. Biophys. Acta **679**:308–314.
25. **Takamiya, S., R. Furushima, and H. Oya.** 1984. Electron transfer complexes of *Ascaris suum* muscle mitochondria. I. Characterization of NADH-cytochrome *c* reductase (complex I-III), with special reference to cytochrome localization. Mol. Biochem. Parasitol. **13**:121–134.
26. **Takamiya, S., K. Kita, H. Wang, P. P. Weinstein, A. Hiraishi, H. Oya, and T. Aoki.** 1993. Developmental changes in the respiratory chain of *Ascaris* mitochondria. Biochim. Biophys. Acta **1141**:65–74.
27. **Thompson, R. C., P. Deplazes, and J. Eckert.** 1990. Uniform strobilar development of *Echinococcus multilocularis* in vitro from protoscolex to immature stages. J. Parasitol. **76**:240–247.
28. **Tielens, A. G. M., C. Rotte, J. J. van Hellemond, and W. Martin.** 2002. Mitochondria as we don't know them. Trends Biochem. Sci. **27**:564–572.
29. **Tielens, A. G. M., and J. J. van Hellemond.** 1998. The electron transport chain in anaerobically functioning eukaryotes. Biochim. Biophys. Acta **1365**: 71–78.
30. **Towbin, H., T. Staehelin, and J. Gordon.** 1979. Electrophoretic transfer of proteins from polyacrylamide gels to nitrocellulose sheets: procedure and some applications. Proc. Natl. Acad. Sci. USA **76**:4350–4354.
31. **van Hellemond, J. J., M. Klockiewicz, C. P. Gaasenbeek, M. H. Roos, and A. G. M. Tielens.** 1995. Rhodoquinone and complex II of the electron transport chain in anaerobically functioning eukaryotes. J. Biol. Chem. **270**: 31065–31070.
32. **Walker, M., J. F. Rossignol, P. Torgerson, and A. Hemphill.** 2004. In vitro effects of nitazoxanide on *Echinococcus granulosus* protoscoleces and metacestodes. J. Antimicrob. Chemother. **54**:609–616.
33. **Wissenbach, U., A. Kroger, and G. Unden.** 1990. The specific functions of menaquinone and demethylmenaquinone in anaerobic respiration with fumarate, dimethylsulfoxide, trimethylamine *N*-oxide and nitrate by *Escherichia coli*. Arch. Microbiol. **154**:60–66.
34. **Wissenbach, U., D. Ternes, and G. Unden.** 1992. An *Escherichia coli* mutant containing only demethylmenaquinone, but no menaquinone: effects on fumarate, dimethylsulfoxide, trimethylamine *N*-oxide and nitrate respiration. Arch. Microbiol. **158**:68–73.
35. **Yamashita, T., T. Ino, H. Miyoshi, K. Sakamoto, A. Osanai, E. Nakamaru-Ogiso, and K. Kita.** 2004. Rhodoquinone reaction site of mitochondrial complex I, in parasitic helminth, *Ascaris suum*. Biochim. Biophys. Acta **1608**: 97–103.

Available online at www.sciencedirect.com
ScienceDirect
Parasitology International 57 (2008) 229–232
www.elsevier.com/locate/parint

Short communication

Mutation underlying resistance of *Plasmodium berghei* to atovaquone in the quinone binding domain 2 (Qo_2) of the cytochrome *b* gene

Josephine E. Siregar [a,d], Din Syafruddin [a,b], Hiroyuki Matsuoka [c], Kiyoshi Kita [d], Sangkot Marzuki [a,*]

[a] *Eijkman Institute for Molecular Biology, Jakarta, Indonesia*
[b] *Department of Parasitology, Faculty of Medicine, Hasanuddin University, Makassar, Indonesia*
[c] *Department of Medical Zoology, Jichi Medical University, Tochigi, Japan*
[d] *Department of Biomedical Chemistry, Graduate School of Medicine, The University of Tokyo, Tokyo, Japan*

Received 7 March 2007; received in revised form 29 November 2007; accepted 1 December 2007
Available online 8 December 2007

Abstract

The anti-malarial agent atovaquone specifically targets the cytochrome bc_1 complex and inhibits the parasite respiration. Resistance to this drug, a coenzyme Q analogue, is associated with mutations in the mitochondrial cytochrome *b* gene. We previously reported atovaquone resistant mutations in *Plasmodium berghei*, in the first quinone binding domain (Qo_1) of the cytochrome *b* gene (M133I and L144S) with V284F in the sixth transmembrane domain. However, in *P. falciparum* the most common mutations are found in the Qo_2 region. To obtain a better model for biochemical and genetic studies, we have now extended our study to isolate a wider range of *P. berghei* resistant strains, in particular those in the Qo_2. Here we report four new mutations (Y268N, Y268C, L271V and K272R), all in the Qo_2 domain. Two of these mutations are convergent to codon 268 (nt802–804) drug-induced mutation in *P. falciparum*.

Keywords: *Plasmodium berghei*; Cytochrome *b* gene mutations; Atovaquone resistance

The emergence of drug-resistant strains of *Plasmodium falciparum* within the last few decades has caused major problems in malaria treatment and control in many endemic countries. New affordable drugs that target different biochemical pathways in the malaria parasite are needed. Atovaquone, a hydroxy-1,4,-naphthoquinone, is an anti-malaria that shares structural similarity with protozoan ubiquinone, a coenzyme involved in the mitochondrial electron transport [1,2]. It is effective against chloroquine-resistant strains of *P. falciparum*, and is a major component of Malarone™ (a fixed combination of atovaquone and proguanil).

This drug collapses mitochondrial membrane potential in *Plasmodium* spp [3], and is suggested to act by competitive binding with ubiquinone at the quinone binding domain of the quinol-cytochrome *c* reductase of the mitochondrial respiratory chain (bc_1 complex, also referred to as complex III). Mutations conferring atovaquone resistance were identified in the mitochondrial cytochrome *b* (*cytb*) gene of *P. berghei* [4], *P. yoelii* [5], *P. falciparum* [6], *Pneumocystis carinii* [7], and *Toxoplasma gondii* [8]. In *Plasmodium* spp, 10 mutations, M133I, L144S, I258M, F267I, Y268C/N/S, L271F/V, K272R, P275T, G280D, and V284F had been documented, mostly located in the quinone binding domain 2 (Qo_2). Significantly, mutations affecting codon 268 (nt802–804) of the *cytb* gene in the Qo_2 domain, have been reported also in *P. falciparum* isolates collected from malaria-infected individuals in Africa, associated with the use of, and in some cases with demonstrated treatment-failure against Malarone [9–11], leading to the suggestion for its use as a molecular marker for atovaquone resistance in the field isolates [12].

The two main *P. berghei* mutations reported previously [4], M133I and L144S, were all located in the quinone binding domain 1 (Qo_1); these mutations confer up to 1000-fold

* Corresponding author. Eijkman Institute for Molecular Biology, Jalan Diponegoro 69, Jakarta 10430, Indonesia. Tel.: +62 21 3917131; fax: +62 21 3147982.
E-mail address: smarzuki@eijkman.go.id (S. Marzuki).

1383-5769/$ - see front matter © 2007 Elsevier Ireland Ltd. All rights reserved.
doi:10.1016/j.parint.2007.12.002

resistance in combination with V284F in the sixth transmembrane domain, which is adjacent to Qo_2 site. To obtain a better model for the biochemical and genetic studies of mutations observed in the human *P. falciparum*, we have now extended our study to isolate a wider range of *P. berghei* resistant strains, in particular those in the Qo_2 region conferring high degrees of resistance. Here we report four new mutations, most in the Qo_2 domain, two of which are convergent to codon 268 mutations in *P. falciparum*.

P. berghei ANKA strains were inoculated intraperitoneally into 10–12 week old BALB/c mice at approx 10^7 parasitized red blood cells/mouse. At the parasitemia level of 1–5%, the *P. berghei*-infected mice were treated intraperitoneally with different doses of atovaquone, between 0.5 and 14.4 mg kg^{-1} BW as specified in Table 1, daily for three consecutive days. Parasites were then allowed to recover for 7 days in the absence of the drug, before the same daily treatment was introduced for another 3 days. This cycle of treatment was repeated until resistance was observed, as indicated by level of parasitemia which was monitored daily. The resistant parasites were then reinoculated intraperitoneally into 10–12 week old BALB/c mice to obtain enough parasites for drug resistance test (legend of Table 1) and cryofreezing. Some isolates were further cloned by serial limiting dilution and reisolation in mice. Ten isolates were obtained, PbLSJ1 to 8 derived from *P. berghei* ANKA Leiden, and PbESJ9 and 10 from *P. berghei* ANKA Edinburgh (Table 1). In addition PbSK2A1Tb was obtained by following two passages of a frozen PbSK2A1T resistant line from our previous study [4].

Table 1
Atovaquone-resistant isolates of *P. berghei*

Isolates[a]	Atovaquone challenge[b] (mg kg^{-1} BW)	Mutation	ED50[c] (mg kg^{-1} BW)	Growth rate[d] (correlation coefficient)
PbLSJ1.1	14.4	Y268N	80	0.61 (0.96)
PbLSJ2.1	14.4	Y268C	5.2	0.86 (0.84)
PbLSJ3.1	14.4	L271V+K272R	16	1.48 (0.96)
PbESJ9	14.4	L271V+K272R	N.D	N.D
PbESJ10	14.4	L271V+K272R	N.D	N.D
PbSK2A1Tb	Previous study [4]	M133I+L271V	4	1.64 (0.84)
PbLSJ6	8	Y268N	N.D	N.D
PbLSJ4	4	Y268N	N.D	N.D
PbLSJ7	4	Y268C	N.D	N.D
PbLSJ5	2	L271V+K272R	N.D	N.D
PbLSJ8	1	L271V+K272R	N.D	N.D
PbL	Control	Wild type	0.01	6.05 (0.93)

[a] PbLSJ1-8 refer to mutants derived from *P. berghei* ANKA Leiden, while PbESJ9-10 from *P. berghei* ANKA Edinburgh. PbSK2A1Tb appeared following two passages of a frozen PbSK2A1T resistant strain isolated in our previous study [4]; Repeated sequencing confirmed the presence of M133I and V284F in the frozen original PbSK2A1T.

[b] The concentrations of atovaquone indicated are those employed in the isolation of resistant mutants, by treating *P. berghei*-infected BALB/c mice in cycles of 3 days of treatment and 7 days of recovery as described in the text.

[c] Drug resistance test was carried out by inoculating parasite isolates intraperitoneally into the 10–12 week old BALB/c mice, and challenging the infected mice with atovaquone at daily doses ranging from 0.001 to 50 mg kg^{-1} BW. Between three and four mice were used per *P. berghei* isolate per dose of atovaquone. Growth of parasites was determined by daily monitoring of parasitemia for 4–6 days. The 50% Effective Dose (ED50) and correlation coefficient values were calculated from the growth rates of each *P. berghei* isolate during the daily treatment with atovaquone, employing the Sigmoidal Regression Wizard.

[d] Growth rate is expressed as % increase in parasitemia day^{-1}.

A region of the 6 kb mitochondrial DNA (mtDNA) of the various *P. berghei* isolates (nt3368–nt5019) was amplified and sequenced. This region spanned the entire *cytb* gene and, therefore, includes the Qo_1 and Qo_2 domains associated with atovaquone resistance mutations [4,5]. A T to A nucleotide substitution at the first base of codon 268 (nt802) was found in three isolates (PbLSJ1.1, PbLSJ4 and PbLSJ6), leading to amino acid change Y268N in the Qo_2 domain (Table 1). Two other isolates carried an A to G substitution at the second base of the same codon (nt803), leading to amino acid change Y268C (PbLSJ2.1 and PbLSJ7). The remaining five isolates were all double mutants, carrying a T to G nucleotide substitution at nt811 and an A to G at nt815, leading to L271V and K272R, respectively. PbSK2A1Tb carried the Qo_1 G to A substitution at nt399, leading to M133I, as observed in its parental PbSK2A1T line [4], and the T to G substitution at nt811 leading to L271V in the Qo_2 domain were confirmed. Interestingly, the transmembrane V284F amino acid change of the parental line PbSK2A1T [4] has apparently disappeared during the two passages in mice.

The level of resistance of four representative isolates was determined *in vivo* as described in Table 1. The ED_{50} for the parental *P. berghei* ANKA line was found to be 0.01 mg atovaquone kg^{-1} BW, PbSJ1.1 (Y268N) showed the highest degree of resistance, with an ED_{50} of 80 mg kg^{-1} BW, while those for PbSJ2 (Y268C) and PbSJ3 (L271V+K272R) were 5.2 and 16 mg kg^{-1} BW, respectively. PbSK2A1Tb that had both Qo_1 and Qo_2 mutations (M133I+L271V) showed similar order of resistance, with an ED_{50} of 4 mg kg^{-1} BW (Table 1).

All of the mutations found in the present study are located in Qo_2 (Fig. 1), the ubiquinol oxidation domain of the cytochrome *b*, where the electron transfer to the iron–sulphur protein, and the consequent charge separation, results in proton translocation. This is in contrast to results of our earlier attempt to isolate atovaquone resistance mutants of *P. berghei* [4], which had lead to mutations in the Qo_1 domain. In the earlier study mutants were isolated by the exposure of the *P. berghei in vivo* to increasing doses of atovaquone, whereas in the present study the parasite was challenged with repeated cycles of exposure and recovery of single doses of the anti-malaria drug. It is possible that the former procedure has allowed the development of perhaps weaker Qo_1 mutants. The latter is closer to the situation in clinical treatment of malaria, and it is thus of interest to observe similar Qo_2 mutations in field isolates of *P. falciparum*(Y268S, Y268N and Y268C) [6,9,11]. Further, the isolation of *P. falciparum* resistant strains *in vitro*, by the exposure of cultured parasites with step-wise increasing doses of atovaquone, resulted in combinations of Qo_1 and Qo_2

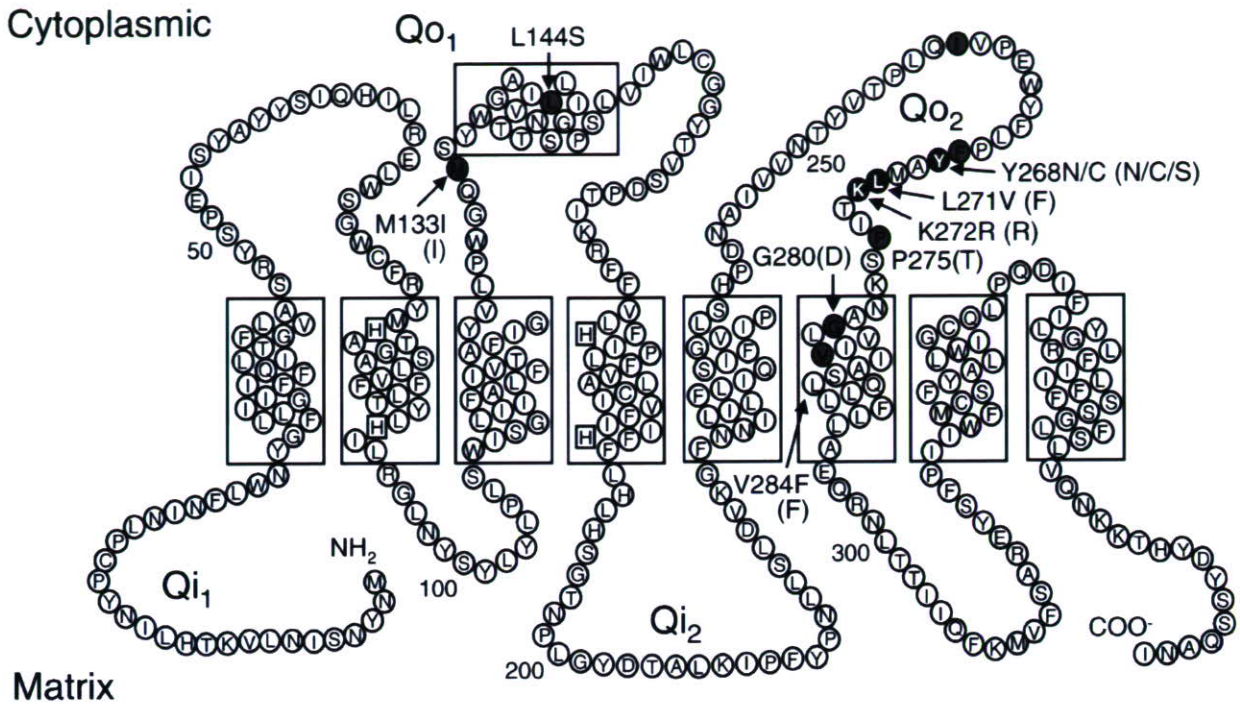

Fig. 1. Sites of atovaquone resistance mutations in the Qo_1 and Qo_2 domains of apocytochrome *b*. The apocytochrome *b* of *P. berghei* contains 376 amino acid residues and 8 transmembrane domains (boxed). Boxed "H"s are the universally conserved histidine residues that act as the axial ligands for b_{566} heme (H78 and H173) and b_{560} heme (H92 and H187). Shown are the four mutations identified in the present study, Y268N, Y268C, L271V, and K272R, all in the quinone binding site II (Qo_2) of the protein. The three atovaquone resistance mutations we reported previously [4] are indicated, M133I and L144S in the quinone binding site I (Qo_1), and V284F in the sixth transmembrane domain. Shown in brackets are mutations reported in *P. falciparum*, i.e. M133I, Y268S, Y268N, Y268C, L271F, K272R, P275T, G280D, and V284F [6,11,12] Other *Plasmodium* atovaquone resistance mutations that had been reported [5,7,8] are indicated as grey shaded residues; in *P. yoelii* these mutations are I258M, F267I, Y268C, L271V and K272R.

mutations (M133I and K272R or P275T), or in transmembrane V284K [6]. The atovaquone resistance conferred by these mutations were between 10 and 100 times lower than that of the field isolates carrying the Y268S mutation. The degree of resistance correlated well with the concentration of atovaquone used in the isolation, and may explain the absence of mutations in codon 268 *in vitro*.

Amino acid residues Y268 and L271 are highly conserved, indicating the potential importance of these residues in maintaining the cytochrome *b* structure and function. Residue 272, on the other hand, is a lysine in *Plasmodium* spp., but is an arginine in vertebrate proteins. Both Y268 and L271 have been suggested to be involved in atovaquone binding in *P. falciparum* cytochrome *b* [6]. Furthermore, in the yeast model [13,14], residues 279 and 282, equivalent to *Plasmodium* residues 268 and 271, have been predicted to be involved in the binding of atovaquone. Site-directed mutagenesis resulting in Y279S and L282V in yeast (corresponding to Y268S and L271V in *Plasmodium*) indeed conferred atovaquone resistance [14].

The two codon 268 mutations found in the present study, Y268N and Y268C, lead to significantly different degrees of resistance (ED_{50} 80 and 5.2, respectively). The aromatic side-chain of the tyrosine at residue 268 is important for the interaction between atovaquone and its binding pocket in the cytochrome *b* [13,14]; site-directed mutations in yeast that remove the aromatic chain gave rise to atovaquone resistance. The substitution of this large hydrophobic residue with the smaller asparagine or cysteine would affect this interaction, and the difference in the polarity of the side chains of the two amino acids could explain the difference in degree of resistance conferred.

We found in the present study that the mutation at codon 271 was always associated with either K272R or M133I. The single mutation, L271V, may lead to a functionally defective structure that requires compensative mutations, either in the adjacent Qo_2 site, 272, or in Qo_1 site, 133, to restore stability. The significantly reduced growth rates of the various atovaquone resistant mutants indeed suggest that there is some disruption of the cytochrome *b* function. The mutations in the atovaquone binding domain could for example affect also the functional interaction between coenzyme Q and the cytochrome *b*. Further biochemical analyses of the *P. berghei* atovaquone resistant clones are in progress to elucidate the structure functional relationship underlying atovaquone resistance, and to examine the fitness of the mutant strains in genetic crosses.

Acknowledgments

The authors wish to thank Dr. Andy Waters, Leiden University Medical Center (LUMC), Netherland, and Dr. A. Kurniawan, Dept. of Parasitology, Faculty of Medicine, University of Indonesia for the gift of *P. berghei* ANKA strains.

This work was supported by a grant from the Indonesian government through the Ministry of Research and Technology and from the Japan Society for the Promotion of Sciences (JSPS) to JES, through a JSPS fellowship for PhD RONPAKU program. This study was also supported by a grant-in-aid for scientific research on Priority Areas, for the 21st Century COE Program (F-3) and for Creative Scientific Research from the Japanese Ministry of Education, Science, Culture, Sports and Technology (180 73004, 18GS0314).

References

[1] Fry M, Pudney M. Site of action of the antimalarial hydroxynaphthoquinone, 2-[trans-4-(4'-chlorophenyl)cyclohexyl]-3-hydroxy-1,4-naphthoquinone(566C80). Biochem Pharmacol 1992;43:1545–53.

[2] Vaidya AB, Lashgari MS, Pologe LG, Morrisey J. Structural features of *Plasmodium* cytochrome *b* that may underline susceptibility to 8-aminoquinolines and hydroxynaphthoquinones. Mol Biochem Parasitol 1993;58:33–42.

[3] Srivastava IK, Rottenberg H, Vaidya AB. Atovaquone, a broad spectrum antiparasitic drug, collapses mitochondrial membrane potential in a malarial parasite. J Biol Chem 1997;272:3961–6.

[4] Syafruddin D, Siregar JE, Marzuki S. Mutations in the cytochrome *b* gene of *Plasmodium berghei* conferring resistance to atovaquone. Mol Biochem Parasitol 1999;104:185–94.

[5] Srivastava IK, Morrisey JM, Darrouzet E, Daldal F, Vaidya AB. Resistance mutations reveal the atovaquone-binding domain of cytochrome *b* in malaria parasites. Mol Microbiol 1999;33:704–11.

[6] Korsinczky M, Chen N, Kotecka B, Saul A, Rieckmann K, Cheng Q. Mutations in *Plasmodium falciparum* cytochrome *b* that are associated with atovaquone resistance are located at a putative drug-binding site. Antimicrob Agents Chemother 2000;44:2100–8.

[7] Walker DJ, Wakefield AE, Dohn MN, Miller RF, Baughman RP, Hossler PA, et al. Sequence polymorphism in the *Pneumocystis carinii* cytochrome *b* gene and their association with atovaquone prophylaxis failure. J Infect Dis 1998;178:1767–75.

[8] McFadden DC, Tomavo S, Berry EA, Boothroyd JC. Characterization of cytochrome *b* from *Toxoplasma gondii* and Q_o domain mutations as a mechanism of atovaquone-resistance. Mol Biochem Parasitol 2000;108:1–12.

[9] Fivelman QL, Butcher GA, Adagu IS, Warhust DC, Pasvol G. Malarone treatment failure and *in vitro* confirmation of resistance of *Plasmodium falciparum* isolate from Lagos, Nigeria. Malaria J 2002;I:1–4.

[10] David KP, Alifrangis M, Salanti A, Vestergaard LS, Ronn A, Bygbjerg IB. Atovaquone/proguanil resistance in Africa: a case report. Scand J Infect Dis 2003;35:897–8.

[11] Musset L, Bouchaud O, Matheon S, Massias L, Le BJ. Clinical atovaquone–proguanil resistance of *Plasmodium falciparum* associated with cytochrome *b* codon 268 mutations. Microbes Infect 2006;11:2599–604.

[12] Schwöbel B, Alifrangis M, Salanti A, Jelinek T. Different mutation patterns of atovaquone resistance to *Plasmodium falciparum in vitro* and *in vivo*: rapid detection of codon 268 polymorphisms in the cytochrome *b* as potential *in vivo* resistance marker. Malaria J 2003;2:1–7.

[13] Kessl JJ, Lange BB, Merbitz-Zahradnik TM, Zwickers K, Hill P, Meunier B, et al. Molecular basis for atovaquone binding to the cytochrome bc_1 complex. J Biol Chem 2003;278:31312–8.

[14] Kessl JJ, Ha KH, Merritt AK, Lange BB, Hill P, Meunier B, et al. Cytochrome *b* mutations that modify the ubiquinol-binding pocket of the cytochrome bc_1 complex and confer anti-malarial drug resistance in *Saccharomyces cerevisiae*. J Biol Chem 2005;280:17142–8.

J|A|C|S
ARTICLES
Published on Web 10/10/2007

Time-Resolved Long-Lived Luminescence Imaging Method Employing Luminescent Lanthanide Probes with a New Microscopy System

Kenjiro Hanaoka,† Kazuya Kikuchi,‡ Shigeru Kobayashi,§ and Tetsuo Nagano*,†

Contribution from the Graduate School of Pharmaceutical Sciences, The University of Tokyo, 7-3-1 Hongo, Bunkyo-ku, Tokyo 113-0033, Department of Materials and Life Sciences, Graduate School of Engineering, Osaka University, 2-1 Yamada-oka, Suita City, Osaka 565-0871, and Products Development Department 2, Micro-Imaging Systems Division, OLYMPUS CORPORATION, 2951 Ishikawa-cho, Hachioji-shi, Tokyo 192-8507, Japan

Received May 13, 2007; E-mail: tlong@mol.f.u-tokyo.ac.jp

Abstract: Superior fluorescence imaging methods are needed for detailed studies on biological phenomena, and one approach that permits precise analyses is time-resolved fluorescence measurement, which offers a high signal-to-noise ratio. Herein, we describe a new fluorescence imaging system to visualize biomolecules within living biological samples by means of time-resolved, long-lived luminescence microscopy (TRLLM). In TRLLM, short-lived background fluorescence and scattered light are gated out, allowing the long-lived luminescence to be selectively imaged. Usual time-resolved fluorescence microscopy provides fluorescence images with nanosecond resolution and has been used to image interactions between proteins, protein phosphorylation, the local pH, the refractive index, ion or oxygen concentrations, etc. Luminescent lanthanide complexes (especially europium and terbium trivalent ions (Eu^{3+} and Tb^{3+})), in contrast, have long luminescence lifetimes on the order of milliseconds. We have designed and synthesized new luminescent Eu^{3+} complexes for TRLLM and also developed a new TRLLM system using a conventional fluorescence microscope with an image intensifier unit for gated signal acquisition and a xenon flash lamp as the excitation source. When the newly developed luminescent Eu^{3+} complexes were applied to living cells, clear fluorescence images were acquired with the TRLLM system, and short-lived fluorescence was completely excluded. By using Eu^{3+} and Tb^{3+} luminescent complexes in combination, time-resolved dual-color imaging was also possible. Furthermore, we monitored changes of intracellular ionic zinc (Zn^{2+}) concentration by using a Zn^{2+}-selective luminescent Eu^{3+} chemosensor, [Eu-7]. This new imaging technique should facilitate investigations of biological functions with fluorescence microscopy, complementing other fluorescence imaging methodologies.

Introduction

Fluorescence imaging is a powerful tool for the visualization of biomolecules in various biological environments and is important for elucidating biological functions.[1,2] Further, the development of new fluorescent dyes with improved photophysical properties combined with technical progress in optical devices for fluorescence microscopy will open the way to superior fluorescence imaging technologies. Usual time-resolved fluorescence microscopy exploits differences in fluorescence lifetimes on the order of nanoseconds to monitor target fluorescence, and this technique has been used to image interactions between proteins or protein phosphorylation by detecting fluorescence resonance energy transfer (FRET) and to report on the local environment of fluorophores, for example, the local pH, the refractive index, ion or oxygen concentrations, etc.[3] In this paper, we present a new system for time-resolved long-lived luminescence microscopy (TRLLM), which utilizes the extremely long luminescence lifetimes of luminescent lanthanide complexes, on the order of milliseconds. This approach is expected to allow imaging with complete elimination of the short-lived background fluorescence,[4-13] providing high signal-to-noise ratios, by the introduction of an appropriate delay

† The University of Tokyo.
‡ Osaka University.
§ OLYMPUS CORPORATION.

(1) Nalbant, P.; Hodgson, L.; Kraynov, V.; Toutchkine, A.; Hahn, K. M. *Science* **2004**, *305*, 1615–1619.
(2) Wang, X.; Weisleder, N.; Collet, C.; Zhou, J.; Chu, Y.; Hirata, Y.; Zhao, X.; Pan, Z.; Brotto, M.; Cheng, H.; Ma, J. *Nat. Cell Biol.* **2005**, *7*, 525–530.
(3) Suhling, K.; French, P. M. W.; Phillips, D. *Photochem. Photobiol. Sci.* **2005**, *4*, 13–22.
(4) Weibel, N.; Charbonnière, L. J.; Guardigli, M.; Roda, A.; Ziessel, R. *J. Am. Chem. Soc.* **2004**, *126*, 4888–4896.
(5) Marriott, G.; Heidecker, M.; Diamandis, E. P.; Marriott, Y. Y. *Biophys. J.* **1994**, *67*, 957–965.
(6) Marriott, G.; Clegg, R. M.; Arndt-Jovin, D. J.; Jovin, T. M. *Biophys. J.* **1991**, *60*, 1374–1387.
(7) Beeby, A.; Botchway, S. W.; Clarkson, I. M.; Faulkner, S.; Parker, A. W.; Parker, D.; Williams, J. A. G. *J. Photochem. Photobiol., B* **2000**, *57*, 83–90.
(8) Phimphivong, S.; Saavedra, S. S. *Bioconjugate Chem.* **1998**, *9*, 350–357.
(9) de Haas, R. R.; van Gijlswijk, R. P. M.; van der Tol, E. B.; Veuskens, J.; van Gijssel, H. E.; Tijdens, R. B.; Bonnet, J.; Verwoerd, N. P.; Tanke, H. J. *J. Histochem. Cytochem.* **1999**, *47*, 183–196.
(10) Vereb, G.; Jares-Erijman, E.; Selvin, P. R.; Jovin, T. M. *Biophys. J.* **1998**, *74*, 2210–2222.

 10.1021/ja073392j CCC: $37.00

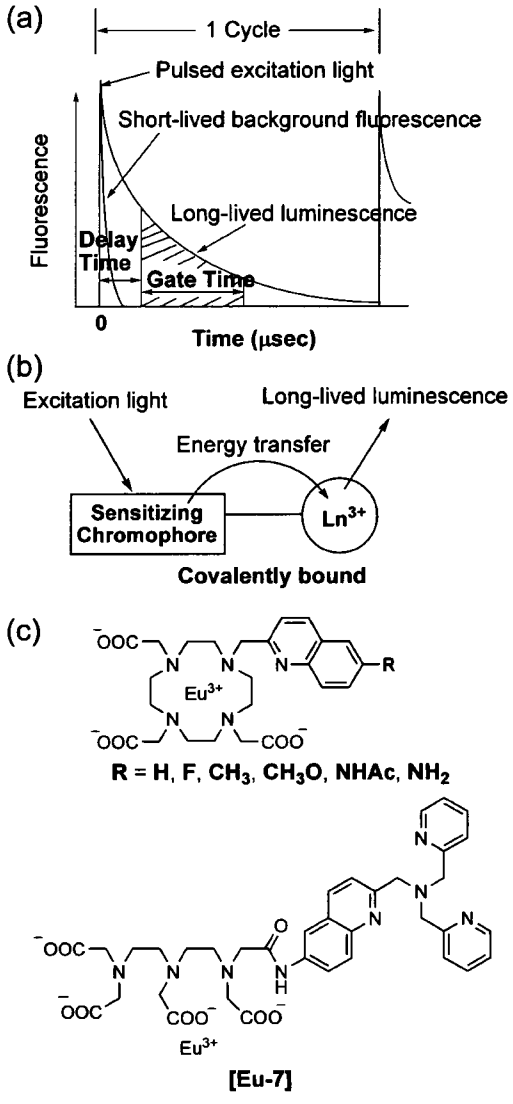

Figure 1. Design of luminescent lanthanide complexes. (a) Principle of time-resolved long-lived luminescence measurements. The short-lived background fluorescence decays to negligible levels during an appropriate *delay time* between a pulse of excitation light and the measurement of the long-lived luminescence. The period for which the fluorescence is measured is the *gate time*. The time-resolved long-lived luminescence measurement obviates the short-lived background fluorescence. (b) Schematic view of a sensitizing chromophore incorporated into a lanthanide emitter. Efficient intramolecular energy transfer should occur from the excited chromophore to the proximate lanthanide ion after excitation of the sensitizing chromophore, and the metal ion becomes excited to the emission state. (c) Structure of the synthesized Eu^{3+}–polyaminocarboxylate complexes incorporating a covalently bound sensitizing chromophore. Eu^{3+} complexes possess various substituents, H, F, CH_3, CH_3O, NHAc, and NH_2, at the 6-position of quinoline (=R) as a light-harvesting moiety for efficient Eu^{3+} sensitization. Also shown is the structure of the Zn^{2+}-selective luminescent Eu^{3+} chemosensor [Eu-7]. Reprinted from ref 29. Copyright 2004 American Chemical Society.

time between the pulsed excitation light and measurement of the long-lived luminescence of the dyes (Figure 1a). Thus, this TRLLM imaging has characteristics very different from those of conventional time-resolved fluorescence imaging.

New fluorescent dyes with a long fluorescence lifetime are needed for the TRLLM-based microscopic method. Typical organic phosphorescent dyes, which possess high triplet quantum yields, such as eosin or erythrosine or metal complexes showing MLCT luminescence are considered to be good candidates for the TRLLM-based microscopic method,[9,14] because phosphorescence lifetimes are relatively long. However, these compounds often transfer the energy of the triplet excited state to surrounding biomolecules in cells and tissues through singlet oxygen, acting as photosensitizers.[14,15] Such light-activated photosensitizing severely limits the use of these phosphorescent dyes in TRLLM, resulting in cell death via apoptosis and/or necrosis and photobleaching of the dyes. Luminescent lanthanide complexes, in particular complexes of europium and terbium trivalent ions (Eu^{3+} and Tb^{3+}), possess extremely long luminescence lifetimes on the order of milliseconds, whereas typical organic fluorescent compounds possess short fluorescence lifetimes in the nanosecond region.[16] Further, luminescent lanthanide complexes are thought to be relatively insensitive to photobleaching and the generation of singlet oxygen compared with phosphorescent dyes.[5] For these reasons, luminescent lanthanide complexes have been recently exploited in various bioassays with time-gating in the fields of medicine, biotechnology, and biological science.[17,18] The lanthanide f–f transitions have low absorbance, so a sensitizing chromophore covalently bound to the ligand is desirable for high luminescence.[16] Absorption by the chromophore results in effective population of its triplet level, and efficient intramolecular energy transfer conveys the absorbance energy of the excited chromophore to a chelated lanthanide metal ion, which becomes excited to the emission state (Figure 1b). Therefore, a proper chromophore design should afford luminescent lanthanide complexes which possess appropriate photochemical properties for TRLLM.[16]

Despite the tremendous amount of work on luminescent lanthanide complexes, only a few complexes have yet been employed for TRLLM,[4,5,7,8,10–13,19–21] and most complexes are used as labeling reagents for proteins. There are numerous requirements to be fulfilled by luminescent lanthanide complexes for usage in molecular imaging with TRLLM, and these include kinetic stability in water and a sensitizing chromophore unit that generates an efficient antenna effect. Further, it would be desirable to move the excitation wavelength toward the visible region to reduce the phototoxicity of the excitation light for biological samples and to ensure compatibility with the optics of standard fluorescence microscopes. Here, we report the design and synthesis of new luminescent Eu^{3+} complexes for use as long-lived luminescent dyes for TRLLM and the development of a new TRLLM system, based on conventional fluorescence

(11) Seveus, L.; Väisälä, M.; Syrjänen, S.; Sandberg, M.; Kuusisto, A.; Harju, R.; Salo, J.; Hemmilä, I.; Kojola, H.; Soini, E. *Cytometry* **1992**, *13*, 329–338.
(12) Sevéus, L.; Väisälä, M.; Hemmilä, I.; Kojola, H.; Roomans, G. M.; Soini, E. *Microsc. Res. Tech.* **1994**, *28*, 149–154.
(13) Connally, R.; Veal, D.; Piper, J. *Microsc. Res. Tech.* **2004**, *64*, 312–322.
(14) Redmond, R. W.; Gamlin, J. N. *Photochem. Photobiol.* **1999**, *70*, 391–475.
(15) Gorman, A.; Killoran, J.; O'Shea, C.; Kenna, T.; Gallagher, W. M.; O'Shea, D. F. *J. Am. Chem. Soc.* **2004**, *126*, 10619–10631.
(16) Parker, D.; Williams, J. A. G. *J. Chem. Soc., Dalton Trans.* **1996**, 3613–3628.
(17) Hemmilä, I.; Webb, S. *Drug Discovery Today* **1997**, *2*, 373–381.
(18) Petoud, S.; Cohen, S. M.; Bünzli, J. C. G.; Raymond, K. N. *J. Am. Chem. Soc.* **2003**, *125*, 13324–13325.
(19) Poole, R. A.; Bobba, G.; Cann, M. J.; Frias, J. C.; Parker, D.; Peacock, R. D. *Org. Biomol. Chem.* **2005**, *3*, 1013–1024.
(20) Song, B.; Wang, G.; Tan, M.; Yuan, J. *J. Am. Chem. Soc.* **2006**, *128*, 13442–13450.
(21) Pandya, S.; Yu, J.; Parker, D. *Dalton Trans.* **2006**, 2757–2766.

microscopy, for molecular imaging in living biological samples. We also confirmed the usefulness of this TRLLM method in cultured living cells.

Results and Discussion

Synthesis of Long-Lived Luminescent Dyes for TRLLM. Various luminescent Eu^{3+} complexes (R = H, F, CH_3, CH_3O, NHAc, and NH_2 in the 6-position of the quinoline) (Figure 1c), which were developed as candidate long-lived luminescent dyes for TRLLM, were synthesized via similar routes to examine their suitability for microscopic measurement, which requires strong luminescence and an excitation wavelength longer than 350 nm (because the optics of standard fluorescence microscopes have only marginal transmittance below 350 nm). The synthetic schemes and detailed descriptions of the synthetic procedures for these Eu^{3+} complexes are shown in the Supporting Information.

Luminescence and Chemical Properties of Synthesized Long-Lived Luminescent Dyes. Quinolines with F, CH_3, and CH_3O in the 6-position (=R) have been reported as efficient sensitizing chromophores for Eu^{3+},[22-24] but the photophysical properties of these Eu^{3+} complexes have not been analyzed well. The integrity of the Eu^{3+} complexes must be maintained in vivo to ensure nontoxicity, because the free metal ion and unchelated chelators are generally more toxic than the complex itself.[25] Chelators such as DTPA (diethylenetriamine-*N*,*N*,*N*′,*N*″,*N*″-pentaacetic acid) and DOTA (1,4,7,10-tetraazacyclododecane-1,4,7,10-tetraacetic acid) have very high stability constant values for lanthanide ion,[25] so we expected that our Eu^{3+} complexes would not have serious toxicity. First, the time-delayed luminescence spectra and UV−vis absorption spectra of these Eu^{3+} complexes were measured in 100 mM HEPES buffer (pH 7.4). When time-delayed luminescence spectra were measured with a delay time of 50 μs and a gate time of 1.00 ms, these Eu^{3+} complexes (except R = NH_2) were highly luminescent (Figure 2a). The luminescence spectra displayed six bands, arising from transitions from the emissive $^5D_0$ level to the $^7F_0$, $^7F_1$, $^7F_2$, $^7F_3$, $^7F_4$, and $^7F_5$ levels of the ground states, respectively.[16] Indeed, aqueous solutions of Eu^{3+} complexes except R = NH_2 showed bright pink luminescence upon excitation with a TLC plate reader lamp (312 nm) (see the Supporting Information). The UV−vis absorption spectra of these Eu^{3+} complexes showed intense absorption bands due to the quinolyl substituent, which is the sensitizing chromophore (Figure 2b,c). Figure 2c shows the normalized absorption spectra of Eu^{3+} complexes (R = H, F, CH_3, CH_3O, NHAc, NH_2) between 280 and 450 nm on the basis of Figure 2b, indicating the comparison between the dominant absorption bands of Eu^{3+} complexes at a concentration of 50 μM in HEPES buffer (pH 7.4). The absorption spectra of Eu^{3+} complexes with R = H, F, and CH_3 showed a peak around 320 nm, and introduction of a CH_3O or NHAc substituent (=R) resulted in an absorption peak at close to 330 nm, tailing out to 370 nm. The absorption spectra of the Eu^{3+} complex with R = NH_2 showed an absorption peak at 352 nm, tailing out to 420 nm. Although the Eu^{3+} complex with R = NH_2 showed the longest absorption wavelength among the synthesized Eu^{3+} complexes, this Eu^{3+} complex did not luminesce at all. The luminescence and chemical properties of Eu^{3+} complexes are listed in Table 1. These Eu^{3+} complexes were dissolved even at 10 mM, so they were highly water-soluble. The luminescence quantum yields (ϕ) of the Eu^{3+} complexes except R = NH_2 are sufficiently large for luminescence detection in fluorescence microscopy.[4,7] The luminescence lifetimes of the above Eu^{3+} complexes except R = NH_2 were approximately 0.60 ms in H_2O and 2.00 ms in D_2O. These values indicate that the number of coordinated water molecules (q value)[27] at the Eu^{3+} ion was

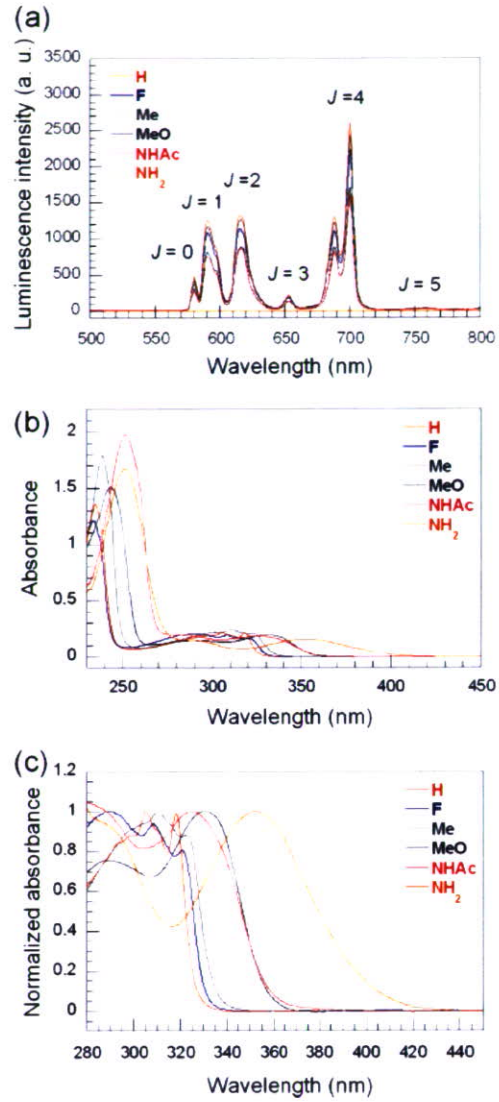

Figure 2. Time-resolved luminescence spectra and absorbance spectra of newly synthesized Eu^{3+} complexes. (a) Time-resolved luminescence spectra of Eu^{3+} complexes (H, red; F, blue; CH_3, green; CH_3O, black; NHAc, pink; NH_2, orange) in HEPES buffer at pH 7.4. The bands arise from $^5D_0 \rightarrow {}^7F_J$ transitions; the J values of the bands are labeled. (b, c) Absorbance spectra of the Eu^{3+} complexes in HEPES buffer at pH 7.4. (b) Absorbance spectra and (c) normalized absorbance spectra over 280 nm. R = H, red; F, blue; CH_3, green; CH_3O, black; NHAc, pink; NH_2, orange.

(22) Griffin, J. M. M.; Skwierawska, A. M.; Manning, H. C.; Marx, J. N.; Bornhop, D. J. *Tetrahedron Lett.* **2001**, *42*, 3823−3825.
(23) Manning, H. C.; Goebel, T.; Marx, J. N.; Bornhop, D. J. *Org. Lett.* **2002**, *4*, 1075−1078.
(24) Kiefer, G. E.; Bornhop, D. J. PCT Int. Appl. WO03/035655 A1, 2003.
(25) Caravan, P.; Ellison, J. J.; McMurry, T. J.; Lauffer, R. B. *Chem. Rev.* **1999**, *99*, 2293−2352.
(26) Nakamaru, K. *Bull. Chem. Soc. Jpn.* **1982**, *55*, 2697−2705.
(27) Beeby, A.; Clarkson, I. M.; Dickins, R. S.; Faulkner, S.; Parker, D.; Royle, L.; de Sousa, A. S.; Williams, J. A. G.; Woods, M. *J. Chem. Soc., Perkin Trans. 2* **1999**, 493−503.

Table 1. Luminescence and Chemical Properties

R	ϕ^a (%)	$\tau_{H_2O}{}^b$ (ms)	$\tau_{D_2O}{}^c$ (ms)	q^d
H	5.9	0.59	2.01	1.14
F	4.2	0.60	1.99	1.10
Me	4.2	0.60	2.00	1.10
MeO	2.4	0.59	1.88	1.10
NHAc	2.6	0.60	1.96	1.09
NH_2	NL[e]	NL	NL	NL

[a] Quantum yields were calculated using $[Ru(bipy)_3]Cl_2$ (bipy = 2,2′-bipyridine; $\phi = 0.028$ in water) as a standard and measured in 100 mM HEPES buffer at pH 7.4, 25 °C.[26] [b] The luminescence lifetimes were measured in H_2O. [c] The luminescence lifetimes were measured in D_2O. [d] q values were estimated using the equation $q^{Eu} = 1.2\ (\tau_{H_2O}{}^{-1} - \tau_{D_2O}{}^{-1} - 0.25)$, which allows for the contribution of unbound water molecules.[27] [e] NL = no luminescence.

approximately 1.10. Thus, the lanthanide hydration state was hardly affected by the introduction of various substituents at the 6-position of the quinolyl sensitizing chromophore of the Eu^{3+} complexes. These results demonstrate that it is feasible to modulate the photophysical properties of Eu^{3+} complexes, such as the intensity of luminescence and the excitation wavelength, and also indicate that the Eu^{3+} complexes with R = NHAc or CH_3O are good candidates for long-lived luminescence dyes for TRLLM because they have a sufficiently long excitation wavelength of over 350 nm.

Time-Resolved Long-Lived Luminescence Imaging in Living Cells. A schematic of the TRLLM system is shown in Figure 3a. This new TRLLM system utilizes a conventional fluorescence microscopy system equipped with an image intensifier (I.I.) unit, a xenon flash lamp, and a timing controller. Applications of mechanical choppers in TRLLM with the use of luminescent lanthanide complexes have been reported by some groups,[4−6,8−12] and some groups have employed an I.I. unit for the time resolution.[7,13] In this study, we used an I.I. unit for the time resolution for the following reasons. First, the gate time (10 μs to 100 ms) and delay time (10 μs to 100 ms) can be easily controlled with the I.I. unit. Second, the I.I. unit improves the uniformity of the emission light, which can be unsatisfactory with mechanical choppers. Third, the gain of the luminescence signal can be adjusted easily. As regards the excitation source, a powerful excitation light is required for time-resolved long-lived luminescence measurements, so a xenon flash lamp was selected. A laser might be preferable, but its wavelength cannot be changed easily.

We examined the application of two Eu^{3+} complexes with R = NHAc or CH_3O to conventional microscopy or TRLLM of cultured living cells (HeLa cells). The fluorescence microscope had an optical window centered at 617 ± 37 nm for the emission due to Eu^{3+}-based luminescence upon excitation at 360 ± 40 nm. The Eu^{3+} complex with R = NHAc or CH_3O was injected into the cultured HeLa cells (Figure 3b). In the prompt fluorescence images, the Eu^{3+} complex-injected cells were seen, together with the Eu^{3+} complex-noninjected cells, which appeared owing to their weak autofluorescence. In the TRLLM images, the autofluorescence from the cells, which is short-lived, was gated out, allowing the Eu^{3+} complex-injected cells to be clearly distinguished.

We next investigated the usefulness of the luminescent Eu^{3+} complexes as long-lived luminescent dyes, since they were expected to have advantages for biological applications. Unlike triplet-state phosphorescent dyes, Eu^{3+} complexes are thought to be insensitive to photobleaching and inefficient generators of singlet oxygen.[5] Reactive oxygen species such as singlet oxygen cause significant cellular damage. First, to evaluate the photostability of Eu^{3+} complexes (R = NHAc or CH_3O), photobleaching experiments with Eu^{3+} complexes and fluorescein were performed in 100 mM HEPES buffer at pH 7.4 (Figure S2, Supporting Information). Fluorescein is often used as a fluorescent dye for fluorescence microscopy. The Eu^{3+} complexes (40 μM) and fluorescein (1 μM) were irradiated with an external light at an appropriate wavelength, 325 nm (1.57 mW) for Eu^{3+} complexes and 492 nm (2.07 mW) for fluorescein. The luminescence intensity of Eu^{3+} complexes (R = NHAc and CH_3O) without time-gating reached 114% and 111% of the initial intensity after 420 min, respectively. The fluorescence intensity of fluorescein was decreased to 48% of the initial intensity after 420 min. The Eu^{3+} complexes appear to be more insensitive to photobleaching than fluorescein. Furthermore, the ability of Rose Bengal, fluorescein, and Eu^{3+} complexes (R = NHAc or CH_3O) to produce singlet oxygen was tested by trapping with 1,3-diphenylisobenzofuran (DPBF), an efficient quencher of singlet oxygen.[15] Rose Bengal is commonly exploited as a photosensitizer and possesses a high triplet quantum yield as a phosphorescent dye.[14] Fluorescein was employed here as a reference sensitizer. The generation of singlet oxygen was evaluated by following the disappearance of the 410 nm absorbance of DPBF at the initial concentration of 20 μM. We used a xenon lamp as a light source and an irradiation wavelength of 555 nm for Rose Bengal, 492 nm for fluorescein, and 325 nm for Eu^{3+} complexes. The values of the relative rate of singlet oxygen generation were 0.89, 0.51, 1, and 18 for Eu^{3+} complexes (R = NHAc and R = CH_3O), fluorescein, and Rose Bengal, respectively (details in Figure S3, Supporting Information). Thus, the Eu^{3+} complexes had relatively low singlet oxygen production, whereas Rose Bengal showed efficient production of singlet oxygen compared with a reference sensitizer, fluorescein.

Dual-Color Imaging with TRLLM. We investigated the feasibility of dual-color imaging with TRLLM using long-lived luminescent Eu^{3+} and Tb^{3+} complexes. Luminescent Tb^{3+} complexes also have advantages for TRLLM, such as long luminescence lifetimes on the order of milliseconds, narrow emission peaks, large Stokes shifts, high quantum yields, and excellent water solubility, like luminescent Eu^{3+} complexes. The main luminescence wavelength of Tb^{3+} complexes is between 480 and 630 nm,[16] and that of Eu^{3+} complexes is between 570 and 720 nm (Figure 2a). The newly synthesized Eu^{3+} complex (R = NHAc) is used as a red emitter, and the Tb^{3+} complex DTPA-cs124 with a chelated Tb^{3+} ion (Tb^{3+}−DTPA-cs124) is employed as a green emitter.[28] This DTPA-cs124 chelator was prepared using the reported procedure,[28] and the complexation of DTPA-cs124 with Tb^{3+} is described in the Supporting Information. The Eu^{3+} complex (R = NHAc) and Tb^{3+}−DTPA-cs124 were injected separately into cultured living HeLa cells. The fluorescence microscope had optical windows centered at 617 ± 37 nm for the Eu^{3+} emission (commercially available Cy3 filter) and at 528 ± 19 nm for the Tb^{3+} emission (commercially available FITC filter) with the same excitation wavelength at 360 ± 40 nm, which also utilized a commercially available filter. In the time-resolved long-lived luminescence

(28) Li, M.; Selvin, P. R. *J. Am. Chem. Soc.* **1995**, *117*, 8132−8138.

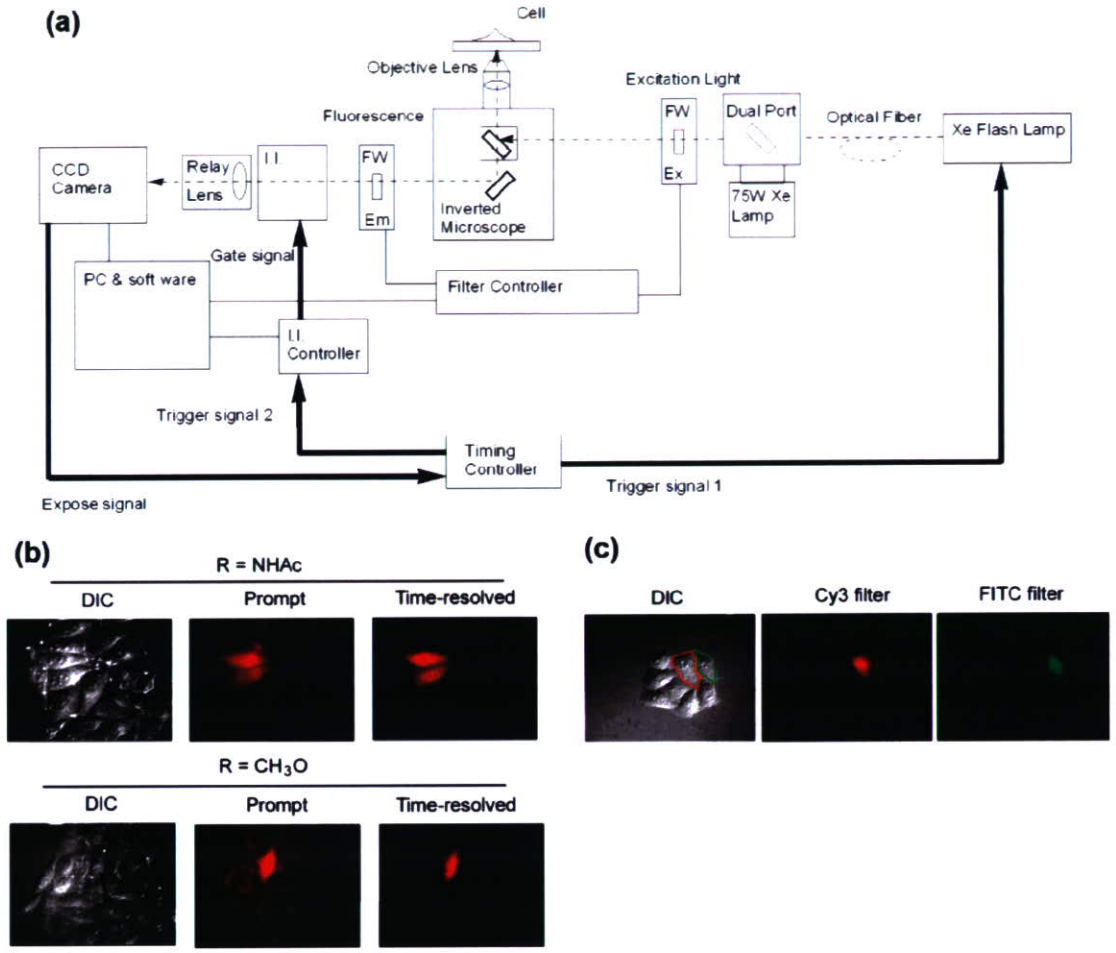

Figure 3. Time-resolved, long-lived luminescence images provided by our new TRLLM system. (a) Schematic diagram of the optical apparatus used for the TRLLM system. The excitation source is a xenon flash lamp. The excitation light passes through the excitation filter and is focused onto cells with dichroic mirrors. The emission light passes through the emission filter. The I.I. unit passes the long-lived luminescence to the CCD camera, controlling the delay time, the gate time, and the gain. The excitation and emission light can be easily selected by using appropriate excitation and emission filters. The image is recorded on the CCD camera and then transferred to the computer for further processing with MetaFluor 6.1 software. (b) One or two cells were injected with the Eu^{3+} complex (R = NHAc or CH_3O) in HBSS buffer. The fluorescence was measured at 617 ± 37 nm, which is the wavelength range of the Cy3 emission filter, with excitation at 360 ± 40 nm. Bright-field transmission images (DIC), prompt fluorescence images (Promp), and time-resolved long-lived luminescence images (Time-resolved) of living cells, including the Eu^{3+} complex-injected cells. (c) Time-resolved dual-color luminescence images of living HeLa cells. One cell was injected with the Eu^{3+} complex (R = NHAc) or Tb^{3+}−DTPA-cs124, respectively. The fluorescence emission at 617 ± 37 nm (the Cy3 emission filter) for Eu^{3+} or 528 ± 19 nm (the FITC emission filter) for Tb^{3+} was measured with excitation at 360 ± 40 nm. DIC: Bright-field transmission image. Red and green colors in DIC show Eu^{3+} complex-injected and Tb^{3+}−DTPA-cs124-injected cells, respectively. Cy3 filter: Time-resolved long-lived luminescence image of DIC with the Cy3 emission filter (617 ± 37 nm). FITC filter: Time-resolved long-lived luminescence image of DIC with the FITC emission filter (528 ± 19 nm).

image produced with the Cy3 filter, the luminescence of Eu^{3+} was clearly seen, whereas that of Tb^{3+} was only weakly detected due to the difference in the range of the emission wavelengths (Figure 3c). With the FITC filter, the Tb^{3+} luminescence was strongly detected, while the Eu^{3+} luminescence was not observed at all (Figure 3c). Thus, our TRLLM technique can provide dual-color detection with appropriate emission filters, in addition to discriminating against short-lived background fluorescence. To our knowledge, this is the first report of dual-color imaging in living cells with TRLLM.

Time-Resolved Long-Lived Luminescence Imaging of Zn^{2+} in Living Cells. We previously reported a Zn^{2+}-selective luminescent Eu^{3+} chemosensor, [Eu-7] (Figure 1c).[29] Zn^{2+} is the second most abundant heavy metal ion after iron in the human body, and chelatable Zn^{2+} plays an important role in various biological systems.[30] This compound, [Eu-7], has a sufficiently long excitation wavelength for fluorescence microscopy and is suitable for fluorescence microscopic measurements of the Zn^{2+} concentration in living cells. In this study, we examined the application of [Eu-7] to cultured living HeLa cells by using our TRLLM system (Figure 4). Optical parameters used for the fluorescence microscope were as follows: the fluorescence microscope had an optical window centered at 617 ± 37 nm for the emission due to Eu^{3+}-based luminescence excited at 360 ± 40 nm. The delay time, prior to initiation of counting, and the gate time, during which counting takes place, were set at 70 and 808 μs, respectively. Compound [Eu-7] was

(29) Hanaoka, K.; Kikuchi, K.; Kojima, H.; Urano, Y.; Nagano, T. *J. Am. Chem. Soc.* **2004**, *126*, 12470−12476.
(30) Vallee, B. L.; Falchuk, K. H. *Physiol. Rev.* **1993**, *73*, 79−118.

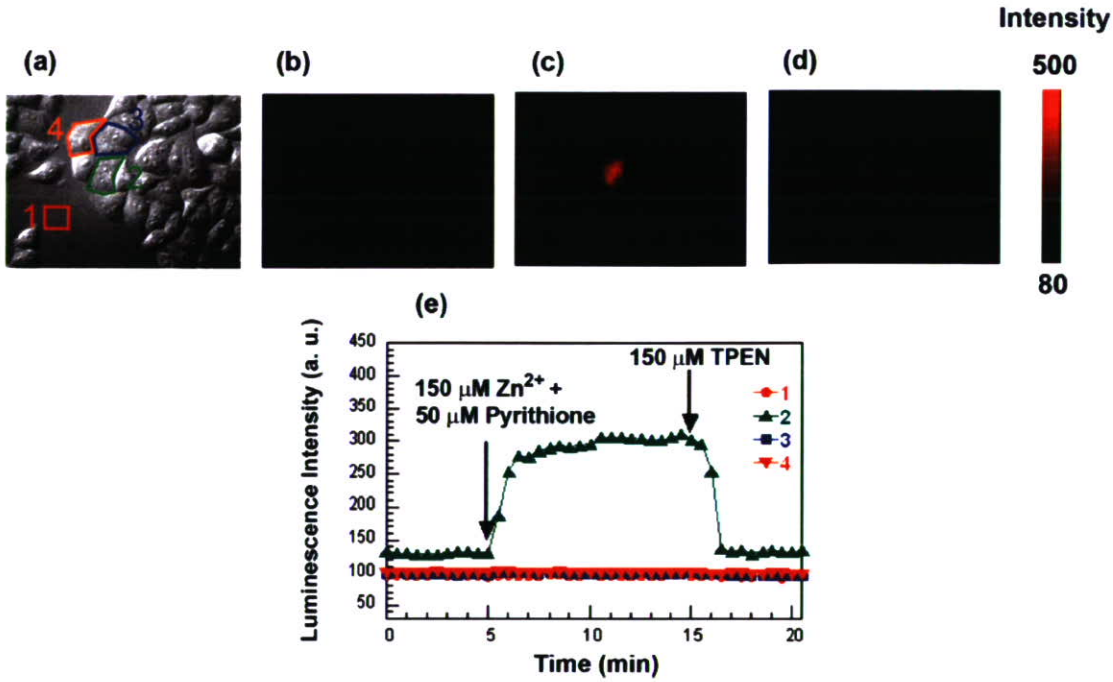

Figure 4. Time-resolved long-lived luminescence imaging of intracellular Zn^{2+} in living HeLa cells. The luminescence at 617 ± 37 nm, excited at 360 ± 40 nm, was measured at 30 s intervals. The time-resolved long-lived luminescence images were measured with our TRLLM system using a delay time of 70 μs and a gate time of 808 μs. The HeLa cells were injected in HBSS buffer with the [Eu-7] solution. (a) Bright-field transmission image (0 min). (b) Time-resolved long-lived luminescence image of (a) (0 min). (c) Time-resolved long-lived luminescence image (7 min) following addition of 5 μM pyrithione (zinc ionophore) and 50 μM $ZnSO_4$ to the medium at 5 min. (d) Time-resolved long-lived luminescence image (17 min) following addition of 100 μM TPEN to the medium at 15 min. Time-resolved long-lived luminescence images (b−d) correspond to the luminescence intensity data in (e), which shows the average intensity of the corresponding area or cell area in (a) (1, extracellular region; 2, intracellular region of the injected cell; 3, 4, intracellular regions of noninjected cells).

injected into a single cultured HeLa cell in the central part of the field of view in Figure 4a,b. A prompt increase of intracellular luminescence was induced when Zn^{2+} (50 μM) and pyrithione (2-mercaptopyridine *N*-oxide, 5 μM), which is a zinc-selective ionophore, were added to the medium at 5 min (Figure 4c). Further, the luminescence intensity decreased immediately upon the extracellular addition of the cell-membrane-permeable chelator TPEN (*N*,*N*,*N*′,*N*′-tetrakis(2-picolyl)ethylenediamine) (100 μM) at 15 min (Figure 4d). Clear images of the intracellular Zn^{2+} concentration changes were obtained with the TRLLM system (Figure 4e). To explore further the utility of TRLLM, we tested whether long-lived luminescence could be well distinguished from the short-lived fluorescence of rhodamine 6G as an artificial source of short-lived background fluorescence. Rhodamine 6G fluorescence directly interferes with Eu^{3+} luminescence because rhodamine 6G has excitation and emission wavelength ranges similar to those of [Eu-7]. As a result, the time-resolved long-lived luminescence images were not affected at all by rhodamine 6G fluorescence (Figure S4, Supporting Information); i.e., [Eu-7] could be used to monitor changes of the intracellular Zn^{2+} concentration even in cells stained with rhodamine 6G.

Conclusions

We have developed a new methodology, i.e., the TRLLM technique with our new luminescent lanthanide complexes, for fluorescence imaging in living biological samples such as live cells. Time-resolved fluorescence imaging has been achieved using other TRLLM systems and luminescent lanthanide complexes, but these complexes were mostly used as labeling reagents for biological molecules. We have shown here that the long-lived luminescence of luminescent lanthanide complexes can be clearly distinguished from the short-lived background fluorescence such as autofluorescence, present in most biological systems as well as scattered excitation light, and even the strong short-lived fluorescence of rhodamine 6G by using our TRLLM system.

By using both luminescent Eu^{3+} and luminescent Tb^{3+} complexes, dual-color imaging was possible with our microscope system. For example, it was possible to discriminate red and green images of luminescent Eu^{3+} and Tb^{3+} complexes with our microscope system using commercially available Cy3 and FITC filters, while excluding short-lived fluorescence. Moreover, we could monitor intracellular Zn^{2+} concentration changes in living cells by using the TRLLM system with our Zn^{2+}-sensitive luminescent lanthanide sensor probe [Eu-7]. This paper is the first to describe imaging of the concentration changes of intracellular metal ion, including Zn^{2+}, in living cells as time-resolved long-lived luminescence images obtained with a luminescent lanthanide sensor probe. The next step should be the development of a range of superior long-lived luminescent lanthanide sensor probes, which possess extremely high quantum yields, long excitation wavelengths over 400 nm, and cell permeability.[31,32] Efforts are under way to develop new long-lived luminescent lanthanide sensor probes which switch between weak and strong luminescence in the absence and the

(31) Yang, C.; Fu, L. M.; Wang, Y.; Zhang, J. P.; Wong, W. T.; Ai, X. C.; Qiao, Y. F.; Zou, B. S.; Gui, L. L. *Angew. Chem., Int. Ed.* **2004**, *43*, 5010−5013.
(32) Allen, M. J.; MacRenaris, K. W.; Venkatasubramanian, P. N.; Meade, T. J. *Chem. Biol.* **2004**, *11*, 301−307.

presence of specific biological molecules, in parallel with efforts to improve our TRLLM system. We consider that our TRLLM imaging technique using luminescent lanthanide sensor probes should be useful as a complement to, rather than a replacement for, existing fluorescence imaging methodologies.

Experimental Section

Materials. DTPA bisanhydride was purchased from Aldrich Chemical Co. Inc. (St. Louis, MO). All other reagents were purchased from either Tokyo Kasei Kogyo Co., Ltd. (Japan) or Wako Pure Chemical Industries, Ltd. (Japan). All solvents were used after distillation. Silica gel column chromatography was performed using BW-300 and Chromatorex-ODS (all from Fuji Silysia Chemical Ltd.).

Instruments. ^{1}H and ^{13}C NMR spectra were recorded on a JEOL JNM-LA300. Mass spectra were measured with a JEOL-T100LC AccuTOF (ESI^+ or ESI^-). HPLC purification was performed on a reversed-phase column (GL Sciences (Tokyo, Japan), Inertsil Prep-ODS 30 mm × 250 mm) fitted on a Jasco PU-1587 system. Time-resolved luminescence spectra were recorded on a Perkin-Elmer LS55 luminescence spectrometer (Beaconsfield, Buckinghamshire, England). The slit width was 5 nm for both excitation and emission. A delay time of 50 μs and a gate time of 1.00 ms were used. UV−vis spectra were obtained on a Shimadzu UV-1650PC (Tokyo, Japan) or an Agilent 8453 (Agilent Technologies, Waldbronn, Germany) UV−vis spectroscopy system. The fluorescence intensities without a delay time were also recorded on a Perkin-Elmer LS55 luminescence spectrometer (Beaconsfield). The slit width was 10 nm for both excitation and emission.

Time-Delayed Luminescence Spectral Measurements. The time-delayed luminescence spectra of Eu^{3+} complexes (50 μM) were measured in 100 mM HEPES buffer at pH 7.4, 24 °C (excitation at 318 nm (R = H), 320 nm (R = F), 323 nm (R = CH_3), 330 nm (R = CH_3O), 325 nm (R = NHAc), and 352 nm (R = NH_2)). The slit width was 5 nm for both excitation and emission. A delay time of 50 μs and a gate time of 1.00 ms were used.

UV−Vis Absorption Spectrum Measurements. The absorption spectra of Eu^{3+} complexes (50 μM) were measured at 24 °C in an aqueous solution buffered to pH 7.4 (100 mM HEPES buffer). UV−vis spectra in Figure 2b,c were recorded on a Shimadzu UV-1650PC.

Quantum Yield Measurements. The luminescence spectra were measured with a Hitachi F4500 spectrofluorometer (Tokyo, Japan). The slit width was 2.5 nm for both excitation and emission. The photomultiplier voltage was 950 V. The luminescence spectra of Eu^{3+} complexes (5 μM) were measured in 100 mM HEPES buffer at pH 7.4, 25 °C, with irradiation at 300 nm. The quantum yields of Eu^{3+} complexes were evaluated using a relative method with reference to a luminescence standard, $[Ru(bpy)_3]Cl_2$ (ϕ = 0.028 in air-equilibrated water).[26] The quantum yields of Eu^{3+} complexes can be expressed by eq 1,[33] where Φ is the quantum yield (subscript "st" stands for the reference and "x" for the sample), A is the absorbance at the excitation wavelength, n is the refractive index, and D is the area (on an energy scale) of the luminescence spectra. The samples and the reference were excited at the same wavelength (300 nm). The sample absorbance at the excitation wavelength was kept as low as possible to avoid fluorescence errors (A_{exc} < 0.03).

$$\Phi_x/\Phi_{st} = [A_{st}/A_x][n_x^2/n_{st}^2][D_x/D_{st}] \quad (1)$$

Luminescence Lifetime Measurements. The luminescence lifetimes of the Eu^{3+} complexes were recorded on a Perkin-Elmer LS-55 luminescence spectrometer (Beaconsfield). The data were collected with 10 μs resolution in H_2O and D_2O and fitted to a single-exponential curve obeying eq 2, where I_0 and I are the luminescence intensities at time t = 0 and time t, respectively, and τ is the luminescence emission lifetime. Lifetimes were obtained by monitoring the emission intensity at 614 nm (λ_{ex} = 318 nm (R = H), 320 nm (R = F), 323 nm (R = CH_3), 330 nm (R = CH_3O), 325 nm (R = NHAc)).

$$I = I_0 \exp(-t/\tau) \quad (2)$$

Determination of the Number of Water Molecules Bound to the Inner Coordination Sphere of Eu^{3+}. The number of coordinated water molecules (q value) at the Eu^{3+} ion is determined by the following equation:[27]

$$q^{Eu} = 1.2(\tau_{H_2O}^{-1} - \tau_{D_2O}^{-1} - 0.25) \quad (3)$$

where τ_{H_2O} or τ_{D_2O} is the luminescence lifetime of the complex in H_2O or D_2O, respectively.

Photobleaching of Eu^{3+} Complexes. Photobleaching of luminescent Eu^{3+} complexes (R = NHAc or CH_3O) (40 μM) and fluorescein (1 μM) was performed in 100 mM HEPES buffer (pH 7.4) at 24 °C by using a xenon lamp (UXL-500D-0, USHIO, Tokyo, Japan) as an excitation source in an SM-5 system (Bunkoh-Keiki Co., Ltd., Tokyo, Japan). The wavelength and the energy of the irradiation light were 325 nm and 1.57 mW for Eu^{3+} complexes and 492 nm and 2.07 mW for fluorescein. The absorbance values of Eu^{3+} complexes (R = NHAc or CH_3O) (40 μM) and fluorescein (1 μM) solution were 0.16 at 325 nm, 0.15 at 325 nm, and 0.08 at 492 nm, respectively. The fluorescence intensities at 618 nm (for Eu^{3+} complexes) and 516 nm (for fluorescein) were recorded on a Perkin-Elmer LS55 luminescence spectrometer (Beaconsfeld) and plotted.

Comparative Singlet Oxygen Generation Measurements. Reaction of 1,3-diphenylisobenzofuran (DPBF) with singlet oxygen was monitored in terms of the reduction in the intensity of the absorbance at 410 nm. An aerated solution of a photosensitizer and DPBF (20 μM) in 100 mM HEPES buffer (pH 7.4)/MeOH = 1/1 was irradiated with a xenon lamp (UXL-500D-0, USHIO) in an SM-5 system (Bunkoh-Keiki Co., Ltd.) at 24 °C. Rose Bengal (1 μM), fluorescein (1 μM), or a Eu^{3+} complex (R = NHAc or CH_3O) (100 μM) was used as a photosensitizer. The wavelength and the energy of the irradiation light were 555 nm and 3.0 mW for Rose Bengal, 492 nm and 3.09 mW for fluorescein, and 325 nm and 2.55 mW for Eu^{3+} complexes (R = NHAc or CH_3O). The UV−vis spectra were recorded on an Agilent 8453 UV−vis spectroscopy system (Agilent Technologies). The absorbance of a Rose Bengal solution (1 μM), a fluorescein solution (1 μM), and Eu^{3+} complex (R = NHAc and CH_3O) solutions without DPBF were 0.08 (at 555 nm), 0.07 (at 492 nm), 0.40 (at 325 nm), and 0.41 (at 325 nm), respectively. Irradiation at 555 or 492 nm of a 20 μM DPBF solution in 100 mM HEPES buffer (pH 7.4)/MeOH = 1/1 produced no change in the intensity of the 410 nm absorption band, which was derived from DPBF. No changes in the absorbance spectra of the photosensitizers were observed during the irradiation, indicating that the photosensitizers were not photobleached in these experiments. However, irradiation at 325 nm of a 20 μM DPBF solution without photosensitizer produced a reduction in the intensity of the 410 nm absorption band of DPBF. Therefore, the rates of oxygenation of a 20 μM DPBF solution without photosensitizer in 100 mM HEPES buffer (pH 7.4)/MeOH = 1/1 on irradiation at 325, 555, or 492 nm were also measured as background rates, and we subtracted the rates of oxygenation of a solution of DPBF (20 μM) only from the rates of oxygenation of a solution of the Eu^{3+} complex (R = NHAc or CH_3O), Rose Bengal, or fluorescein containing DPBF (20 μM) when irradiated at 325 nm (for Eu^{3+} complexes), 555 nm (for Rose Bengal), or 492 nm (for fluorescein). Details are shown in the Supporting Information.

Preparation of Cells. HeLa cells were cultured in Dulbecco's modified Eagle's medium (DMEM) (Invitrogen Corp., Carlsbad, CA), supplemented with 10% fetal bovine serum (Invitrogen Corp.), 1% penicillin, and 1% streptomycin (Invitrogen Corp.) at 37 °C in a 5% CO_2/95% air incubator. The cells were grown on an uncoated 35 mm

(33) Chen, Q. Y.; Feng, C. J.; Luo, Q. H.; Duan, C. Y.; Yu, X. S.; Liu, D. J. *Eur. J. Inorg. Chem.* **2001**, 1063−1069.

diameter glass-bottomed dish (MatTek, Ashland, MA) and washed twice with Hank's balanced salt solution (HBSS) buffer (Invitrogen Corp.), and then the medium was replaced with HBSS buffer before imaging. The Eu^{3+} complexes (2 or 10 mM) were dissolved in microinjection buffer (HBSS buffer) and injected into cells with an Eppendorf injection system (Transjector 5246).

Prompt Fluorescence Microscopy and Imaging Methods. The imaging system consisted of an inverted microscope (IX71, Olympus) with a cooled CCD camera (Cool Snap HQ; Roper Scientific, Tucson, AZ). The microscope was equipped with a xenon lamp (AH2-RX, Olympus), a 40× objective lens (UApo 40× oil/340, NA 1.35; Olympus), and a dichroic mirror (420DCLP, Omega). The whole system was controlled using MetaFluor 6.1 software (Universal Imaging, Media, PA). The fluorescence microscope had an optical window centered at 617 ± 37 nm (S617/73m, Chroma) for the emission due to Eu^{3+}-based luminescence upon excitation at 360 ± 40 nm (D360/40×, Chroma).

TRLLM and Imaging Methods. For time-resolved long-lived luminescence imaging we used the above conventional fluorescence microscopy system with the following modifications, as shown in Figure 3a. The microscope was equipped with an auxiliary 50 Hz pulsed excitation source (60 W xenon flash lamp (L6784), Hamamatsu Photonics K. K., Shizuoka, Japan) triggered by a timing controller (model 555-2C, BNC (Berkeley Nucleonics Corp.)). The delay time and gate time were controlled by an I.I. and I.I. controller (C9016-02, Hamamatsu Photonics K. K.) located in the emission light pathway and synchronized with the xenon flash lamp using a timing controller. The excitation light was delivered into a dual port (U-DPLHA; Olympus, Tokyo, Japan) via an optical fiber (A7632, Hamamatsu Photonics K. K.). The excitation source was easily switched from a xenon flash lamp to a xenon CW lamp. The I.I. device can strongly amplify the fluorescence signal. The amplified emission signal was delivered via a relay lens (A4539, Hamamatsu Photonics K. K.) to a cooled CCD camera (Cool SNAP HQ, Roper Scientific). Time-resolved long-lived luminescence images were acquired with a 52 or 70 μs delay time between the application of a pulse of excitation light to the sample and the acquisition of the luminescence signal, while no delay was used for the acquisition of prompt fluorescence images; to obtain a good signal-to-noise ratio, the overall acquisition time for each image was 1 s. The gate time, which is the acquisition time of the luminescence signal, was 808 μs. Quantitative evaluation of the luminescence images was done using the MetaFluor imaging analysis software package (Universal Imaging Corp.).

Time-Resolved Dual-Color Imaging Methods. The synthesized luminescent Eu^{3+} complex (R = NHAc) (10 mM) or Tb^{3+}–DTPA-cs124 (2 mM) was dissolved in microinjection buffer (HBSS buffer) and injected into cultured living HeLa cells in HBSS buffer. A delay time of 70 μs and a gate time of 808 μs were used. An optical window centered at 528 ± 19 nm (S528/38m, Chroma) was employed for Tb^{3+}-based luminescence.

Time-Resolved Long-Lived Luminescence Imaging of Intracellular Zn^{2+} in Living Cultured HeLa Cells. A Zn^{2+}-selective luminescent Eu^{3+} chemosensor, [Eu-7] (2 mM), was dissolved in microinjection buffer (HBSS buffer) and injected into living HeLa cells. The time-resolved long-lived luminescence images were acquired every 30 s. A delay time of 70 μs and a gate time of 808 μs were used.

Rhodamine 6G Loading Conditions and Imaging Method. HeLa cells were grown on an uncoated 35 mm diameter glass-bottomed dish (MatTek, Ashland, MA) and washed twice with HBSS buffer (Invitrogen Corp.); then the cells were incubated with rhodamine 6G (4 μM) in HBSS buffer for dye loading for 30 min at room temperature, which was a sufficient time for intracellular accumulation of rhodamine 6G judging from the fluorescence seen in the intracellular regions (Figure S4b). The stained cells were washed twice with HBSS buffer, and the medium was replaced with HBSS buffer before imaging. Then [Eu-7] was injected into a cultured living HeLa cell in the same manner as the above experimental method of time-resolved long-lived luminescence imaging of intracellular Zn^{2+} in living cultured HeLa cells. The fluorescence microscope had an optical window centered at 617 ± 37 nm (S617/73m, Chroma) for the emission due to rhodamine 6G-based fluorescence upon excitation at 360 ± 40 nm (D360/40×, Chroma). In time-resolved long-lived luminescence imaging, images with a delay time of 70 μs were free of contributions from prompt fluorescence of rhodamine 6G, while a delay time of 52 μs was not sufficiently long to eliminate this prompt fluorescence from the time-resolved long-lived luminescence images.

Acknowledgment. This work was supported by the Ministry of Education, Culture, Sports, Science and Technology of Japan (Grants for The Advanced and Innovational Research Program in Life Sciences, 16370071 and 16659003 to T.N., 15681012, 17035019, 17036012, 017048006, and 17651119 to K.K.). T.N. was also supported by the Hoh-ansha Foundation. K.K. was also supported by the Sankyo Foundation, by the Kanagawa Academy of Science, and by the Suzuken Memorial Foundation. K.H. was the recipient of Research Fellowships of the Japan Society for the Promotion of Science for Young Scientists.

Supporting Information Available: Detailed descriptions of synthetic procedures for luminescent Eu^{3+} complexes and the luminescent Tb^{3+} complex, photograph of solutions of luminescent Eu^{3+} complexes, photobleaching profiles of solutions of Eu^{3+} complexes and fluorescein, comparative singlet oxygen generation plots of Rose Bengal, fluorescein, and Eu^{3+} complexes, and time-resolved long-lived luminescence images of intracellular Zn^{2+} in HeLa cells which were stained with rhodamine 6G. This material is available free of charge via the Internet at http://pubs.acs.org.

JA073392J

DOI: 10.1002/chem.200700785

A Gd^{3+}-Based Magnetic Resonance Imaging Contrast Agent Sensitive to β-Galactosidase Activity Utilizing a Receptor-Induced Magnetization Enhancement (RIME) Phenomenon

Kenjiro Hanaoka,[a] Kazuya Kikuchi,[b] Takuya Terai,[a] Toru Komatsu,[a] and Tetsuo Nagano*[a]

Abstract: Magnetic resonance imaging (MRI) permits noninvasive three-dimensional imaging of opaque organisms. Gadolinium (Gd^{3+}) complexes have become important imaging tools as MRI contrast agents for MRI studies, though most of them are nonspecific and report solely on anatomy. Recently, MRI contrast agents have been reported whose ability to relax water protons is triggered or greatly enhanced by recognition of a particular biomolecule. This new class of MRI contrast agents could open up the possibility of reporting on the physiological state or metabolic activity deep within living specimens. One possible strategy for this purpose is to utilize the increase in the longitudinal water proton r_1 relaxivity that occurs upon slowing the molecular rotation of a small paramagnetic complex, a phenomenon which is known as receptor-induced magnetization enhancement (RIME), by either binding to a macromolecule or polymerization of the agent itself. Here we describe the design and synthesis of a novel β-galactosidase-activated MRI contrast agent, the Gd^{3+} complex **[Gd-5]**, by using the RIME approach. β-Galactosidase is commonly used as a marker gene to monitor gene expression. This newly synthesized compound exhibited a 57% increase in the r_1 relaxivity in phosphate-buffered saline (PBS) with 4.5% w/v human serum albumin (HSA) in the presence of β-galactosidase. Detailed investigations revealed that RIME is the dominant factor in this increase of the observed r_1 relaxivity, based on analysis of Gd^{3+} complexes **[Gd-5]** and **[Gd-8]**, which is generated from **[Gd-5]** by the activity of β-galactosidase, and spectroscopic analysis of their corresponding Tb^{3+} complexes, **[Tb-5]** and **[Tb-8]**.

Keywords: biosensors · gadolinium complexes · lanthanides · luminescence · magnetic resonance imaging

Introduction

Magnetic resonance imaging (MRI) is a noninvasive imaging technique that can provide images of intact, opaque organisms in three dimensions, even deep within a specimen, without photobleaching or light scattering which are often observed in light-based microscopy imaging experiments.[1] Therefore, MRI is useful not only in clinical medicine, but also in experimental research.[1,2] Nowadays, there is a considerable interest in MRI contrast agents, which can improve the resolution of MR images.[1,2] The MR images are based upon the NMR signal from water protons, and the signal intensity depends upon the water concentration and relaxation time (T_1 and T_2).[2] Paramagnetic ions like the gadolinium ion (Gd^{3+}), primarily shorten the T_1 (spin–lattice) relaxation time with high efficacy by rapid exchange of inner-sphere water molecules with bulk solvent.[3] Thus, Gd^{3+}-based MRI contrast agents increase tissue contrast by increasing water proton relaxation, and are widely used in clinical diagnostics.[4] In Gd^{3+}-based MRI contrast agents, chelation of Gd^{3+} is required for safety reasons: Dissociation of Gd^{3+} from a MRI contrast agent is undesirable, as both the free metal and unchelated ligands are generally more toxic than the complex itself.[2,4] Commonly used MRI

[a] Dr. K. Hanaoka, T. Terai, T. Komatsu, Prof. Dr. T. Nagano
Graduate School of Pharmaceutical Sciences
The University of Tokyo
7-3-1, Hongo, Bunkyo-ku, Tokyo 113-0033 (Japan)
Fax: (+81) 3-5841-4855
E-mail: tlong@mol.f.u-tokyo.ac.jp

[b] Prof. Dr. K. Kikuchi
Department of Materials and Life Sciences
Graduate School of Engineering, Osaka University
2-1 Yamada-oka, Suita City, Osaka 565-0871 (Japan)

Supporting information for this article is available on the WWW under http://www.chemeurj.org/ or from the author.

